SEDIMENTOLOGY the journal of the International Association of Sedimentologists IAS

Sedimentology (2026) doi: 10.1111/sed.70095

Sedimentological controls on the distribution and geometry of chlorite-coated intervals in deeply buried tide-influenced sandstones, Tilje Formation, Norwegian Continental Shelf

LUCIE ALAIN* , CHRISTIAN HAUG EIDE* , HENRIK NYGAARD HANSEN†, AGUSTIN ARGÜELLO SCOTTI‡, MONIKA SHUKLA† , BJØRN TERJE OFTEDAL§, IAN SHARP‡ and ALLARD MARTINIUS§,¶

**Department of Earth Science, University of Bergen, P.O. box 7803 N-5020, Bergen, Norway (E-mail: lucie.alain@uib.no)*

†Department of Geosciences, University of Oslo, P.O. Box 1047 Blindern NO-0316, Oslo, Norway

‡Equinor ASA, Postboks 7200 5020, Bergen, Norway

§Equinor ASA, Arkitekt Ebbells veg 10, Rottvoll 7041, Trondheim, Norway

¶Department of Geoscience and Engineering, Delft University of Technology, Stevinweg 1 2628 CN, Delft, the Netherlands

Associate Editor – Marcos Aurell

ABSTRACT

Chlorite-coated intervals occurring in deeply buried sandstone reservoirs preserve porosity and permeability by inhibiting quartz cementation. However, the geometry of such chlorite-coated intervals and the controls on their distribution remain unclear. The Lower Jurassic Tilje Formation of the Halten Terrace, Norwegian Continental Shelf, shows sparsely distributed chlorite coats preserving high permeability at great depth. Changes between chlorite-coated and quartz-cemented intervals can occur at a centimetre scale and are thus hard to predict. In this study, detailed sedimentological investigations of 12 wells in the Smørbukk Field, integrated with biostratigraphic data and combined with permeability analysis of more than 5000 core plug samples, facilitate the interpretation of depositional elements and the tracing of chlorite-coated intervals across the field. Ten depositional environments are recognised, representing deposition as a large tide-dominated delta that prograded in an embayment for most of the Tilje Formation. A shift in depositional processes occurs towards the top of the formation, with the development of a latest Pliensbachian candidate relative sea-level fall and incision rapidly followed by the onset of a latest Pliensbachian–earliest Toarcian transgressive phase. The transgressive phase is associated with a change to an open-marine seaway and the deposition of marine tidal dunes. Two types of chlorite-coated intervals occur: (i) thick (20 to 30 m), stratigraphically bounded intervals and (ii) thin (<3 m), sparsely distributed intervals. Chlorite-coated intervals occur mostly in fluvial-tidal channels but also occasionally in other depositional environments, suggesting that sedimentological controls do not fully explain their distribution. Instead, regional controls such as the composition of the hinterland, climate, relative sea-level change, tectonics and geochemical conditions in the primary depositional environments are considered important factors. This study illustrates the various geometries of chlorite-coated intervals in the subsurface, having important implications for building predictive models of their distribution and for conventional and CO_2 reservoir characterisation.

Keywords Chlorite-coating, delta, Lower Jurassic, Norwegian Continental Shelf, permeability, quartz cementation, tide-dominated seaway, Tilje Formation.

INTRODUCTION

Porosity and permeability in sandstone reservoirs typically decrease as pressure and thermal stress increase with burial depth due to diagenetic processes like compaction and extensive quartz cementation (Ramm, 1992; Ramm & Bjørlykke, 1994; Walderhaug, 1996). Therefore, the preservation of porosity and permeability in deeply buried (>2.5 km) sandstone reservoirs depends on property-preserving mechanisms, such as the occurrence of grain-coating chlorite that can inhibit quartz cementation by limiting the epitaxial growth of quartz in intergranular space (Heald & Larese, 1974; Ehrenberg, 1993; Bloch *et al.*, 2002; Billault *et al.*, 2003). This may result in abnormally high permeability and porosity preservation at great burial depths (Ehrenberg, 1993; Martinius *et al.*, 2005; Griffiths *et al.*, 2021). Additionally, chlorite has the potential to mineralise with CO_2, which makes it particularly promising for permanent CO_2 sequestration projects (Pham *et al.*, 2011; Sundal & Hellevang, 2019; Cheng *et al.*, 2022). Despite this, the occurrence and distribution of chlorite in the subsurface remain poorly documented, and the controls on the formation of chlorite are not well understood (e.g., Worden *et al.*, 2020).

Chlorite coats occurring in deeply buried sandstone reservoirs can originate from: (i) thermally driven recrystallisation of precursor clay coats such as berthierine (Ehrenberg, 1993; Aagaard *et al.*, 2000; Ajdukiewicz *et al.*, 2010); or (ii) *in situ* precipitation following the dissolution of iron-rich detrital or diagenetic minerals through interaction with pore fluids (Bloch *et al.*, 2002; Worden & Morad, 2003). Recent studies in modern systems have focused on linking the distribution of precursor clay coats with primary depositional environments (Wooldridge *et al.*, 2017, 2018; Griffiths *et al.*, 2019; Virolle *et al.*, 2019a). Additionally, a limited number of studies have attempted to investigate the occurrence of clay coats in ancient analogues and identified depositional environments in which chlorite coats preferably occur (i.e., tidal-fluvial bars; Griffiths *et al.*, 2021; Virolle *et al.*, 2019b). Despite this, the spatial distribution of chlorite-coated intervals in the subsurface has not been investigated in a systematic manner previously. Therefore, the geometry and dimensions of such chlorite-coated intervals, and the controls on their occurrence remain uncertain, representing a significant challenge with regard to the accurate prediction of reservoir quality and development, and the building of reservoir models.

This study investigates the Lower Jurassic Tilje Formation of the Halten Terrace, on the Mid-Norwegian Continental Margin (Figs 1 to 3) from which chlorite coats have been documented down to ca. 6 km depth (Ehrenberg, 1993; Ehrenberg *et al.*, 1998; Martinius *et al.*, 2005; Griffiths *et al.*, 2021; Nichols *et al.*, 2025). In the Smørbukk Field, the succession is buried up to ca. 5 km and porosity and permeability are low (typically 5% to 10% porosity and permeability <1 mD) except in zones where chlorite coats occur, preserving high porosity and permeability (typically 15% to 20% porosity and permeability >50 mD, and occasionally up to 4500 mD at 4.5 km depth). Such chlorite-coated intervals can be easily traced in cores (under white and UV lights) because of their high friability and their brown colour, which contrasts with the more consolidated, quartz-cemented intervals (Fig. 4). Changes between chlorite-coated and quartz-cemented intervals can occur at a centimetre scale, at the well, field and basin scales, and are thus hard to predict. Therefore, only detailed sedimentological investigations combined with petrophysical and petrographic analyses can provide insights into the distribution of chlorite-coated intervals.

The Tilje Formation consists of tide-influenced shallow-marine successions deposited in an epicontinental seaway (Martinius *et al.*, 2001). Although the highly heterolithic nature of the formation has long been a challenge in its investigation, the facies and depositional environments of the Tilje Formation in the Smørbukk Field have been thoroughly studied (Martinius *et al.*, 2001, 2005; Ichaso & Dalrymple, 2014; Ichaso *et al.*, 2016; Griffiths *et al.*, 2021). Despite this, there are conflicting models for the depositional environment of the Tilje Formation (i.e., tide-dominated to mixed-processes estuarine to deltaic succession;

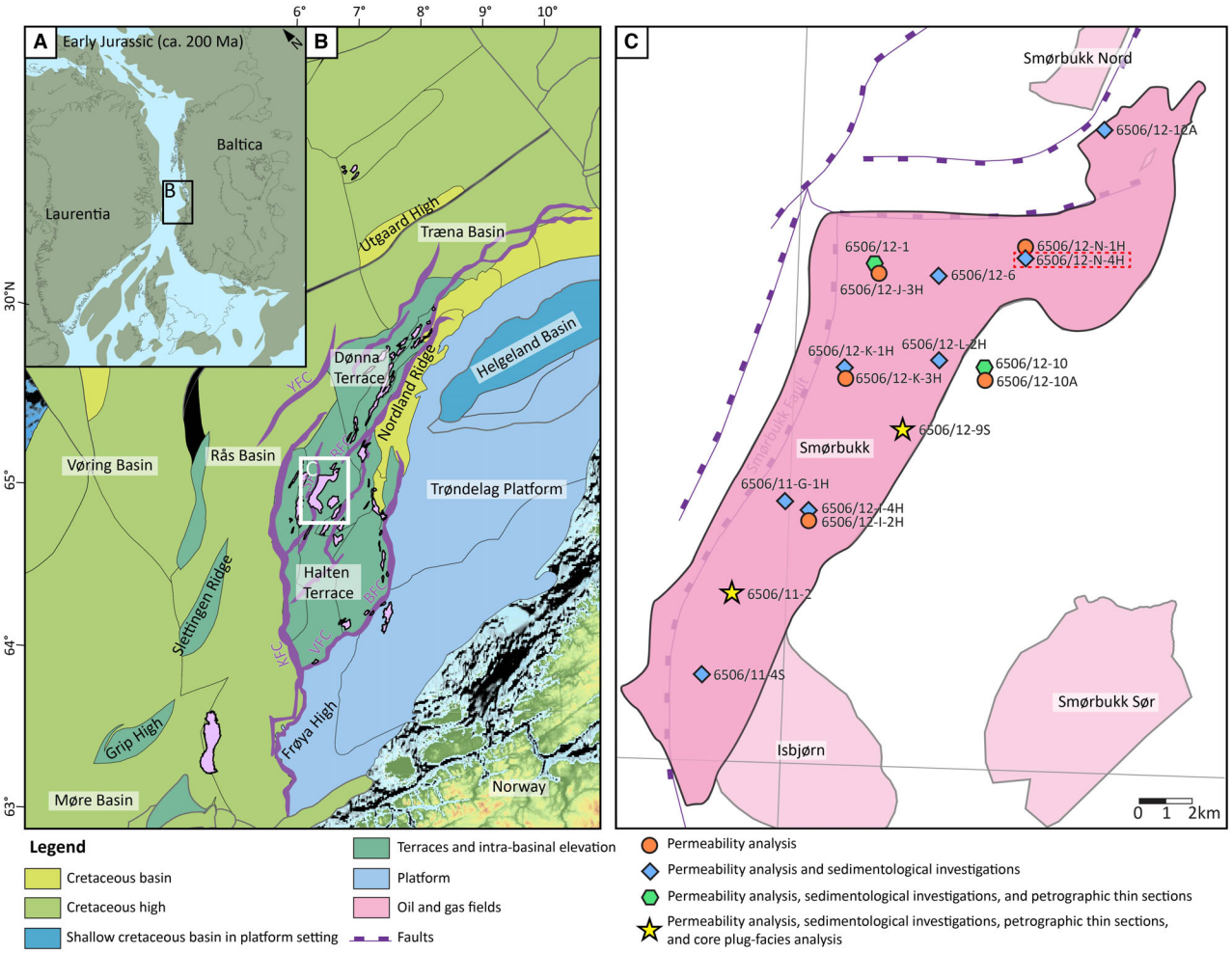

Fig. 1. Location maps showing (A) paleogeographic reconstruction of northern Europe at ca. 200 Ma, adapted from Blakey (2021). (B) Main structural elements of the study area (SODIR, 2025) after Blystad *et al.* (1995) and Bunkholt *et al.* (2025) with background bathymetric map (GEBCO, 2024). BFC, Bremstein Fault Complex; KFC, Klakk Fault Complex; RFC, Revfallet Fault Complex; SF, Smørbukk Fault; VFC, Vingleia Fault Complex; YFC, Ytterholmen Fault Complex. (C) the Smørbukk Field and studied wells with symbols representing the type of analysis and data (SODIR, 2025). Red stippled square highlights the well-investigated in Griffiths *et al.* (2021) and Nichols *et al.* (2025).

Martinius *et al.*, 2001; Ichaso & Dalrymple, 2014) and for sediment provenance and pathways (c.f., Ichaso *et al.*, 2016; Bunkholt *et al.*, 2025). These contrasting models reflect the great regional variability in depositional architecture of the formation and the need for more detailed sedimentological investigations. Additionally, significant progress has been made in the understanding of tide-influenced successions in recent years, especially on the interplay between tidal, fluvial and wave processes (Olariu, 2014; Dalrymple *et al.*, 2015; Gugliotta *et al.*, 2016, 2017; Rossi & Steel, 2016; van Cappelle *et al.*, 2016; Rossi *et al.*, 2017). Therefore, this study aims to reinvestigate the sedimentology of the Tilje Formation in the Smørbukk Field, where the data coverage is excellent (Fig. 1), using sedimentological, ichnological and palynological data, coupled with mapping of the vertical and lateral extent of high-permeability anomalies, to particularly investigate the distribution of chlorite-coated intervals.

The aims of this study are thus the following: (i) to investigate the sedimentology of the Tilje Formation in the Smørbukk Field; (ii) to investigate the distribution and geometry of high permeability anomalies occurring in the study area; (iii) to demonstrate that these anomalies are linked to the occurrence of

chlorite coats; and (iv) to investigate the sedimentological controls on these high permeability anomalies.

GEOLOGICAL SETTING

Structural setting

The Halten Terrace is located in the Norwegian Sea, offshore mid-Norway. It is part of the Norwegian Continental Shelf (NCS), is situated between the Rås Basin to the west and the Trøndelag Platform to the east (Fig. 1), and gradually merges into the Dønna Terrace to the north (Blystad *et al.*, 1995). The Smørbukk Field, the focus of this study, lies centrally in the Halten Terrace and is bounded to the west by the Smørbukk Fault and to the east by the Trestakk Fault (Figs 1 and 3).

The structural development of the Halten Terrace is linked to the evolution of the Norwegian Continental Margin. Following the Caledonian Orogeny, the Norwegian Continental Margin experienced several extensional episodes that ultimately led to the opening of the North Atlantic in the early Eocene (e.g., Doré *et al.*, 1999; Faleide *et al.*, 2008). Five major regional rifting episodes that reactivated Caledonian basement structures occurred between the Devonian and the Eocene (e.g. Blystad *et al.*, 1995; Doré *et al.*, 1999). In the late Permian to Early Triassic, a major rift event led to fault-block rotation and tectonic activity along existing faults (Müller *et al.*, 2005). This was followed by a second rift phase in the Middle to Late Triassic and by marine flooding and deposition of evaporite successions (Müller *et al.*, 2005; Bunkholt *et al.*, 2025). These evaporites later acted as a detachment zone and facilitated thin-skinned tectonic processes that controlled the development of the Halten and Dønna terraces (Marsh *et al.*, 2010; Bunkholt *et al.*, 2025). During the Early to Middle Jurassic, a super-regional transgression and warming climate resulted in the widespread deposition of shallow-marine sediments which accumulated on the Halten and Dønna terraces and the Trøndelag Platform and formed largely tabular stratigraphic units. In the latest Pliensbachian to early Toarcian, however, tectonic activity was locally rejuvenated, resulting in limited local fault-block rotation and intrabasinal erosion within the uppermost Tilje or around the boundary between the Tilje and Ror formations (Bunkholt *et al.*, 2025). A third major rifting event during the Middle Jurassic to Early Cretaceous was associated with accelerated tectonic processes and deep erosion of the uplifted intrabasinal highs. During this rifting phase, faulting along the Bremstein and Vingleia Fault Complexes ultimately led to the detachment of the Halten and Dønna Terraces from the Trøndelag Platform (Blystad *et al.*, 1995).

Stratigraphic setting

The Pliensbachian to Toarcian-aged Tilje Formation is part of the Early Jurassic Båt Group, comprising four formations that overlay the Triassic Upper Grey Beds (Fig. 2). The lower boundary of the group is defined below the first coal bed of the Åre Formation, which consists of coal-bearing floodplain and interdistributary bay-fill, wave- and tide-influenced estuarine, and shoreface deposits towards the top (Dalland *et al.*, 1988; Thrana *et al.*, 2014). The base of the Tilje Formation is defined as a first erosive-based sandstone bed overlying the fine-grained wave-dominated deposits of the uppermost Åre Formation (Ichaso *et al.*, 2016). The Tilje Formation, the focus of this study, is characterised by interbedded highly heterolithic sandstones and mudstones deposited in fluvial-tidal deltaic settings in a narrow seaway (Martinius *et al.*, 2001). The succession has been previously divided into two stratigraphic sequences (sequences 2 and 3; Fig. 2) interpreted as representing a tide-dominated estuarine fill and a fluvial- to tidal-influenced delta (Martinius *et al.*, 2001), or mixed-energy deltaic deposits influenced by subtle tectonic activity (Ichaso & Dalrymple, 2014). The Tilje Formation is sharply overlain by the open-marine mudstone deposits of the Ror Formation. The Ror Formation occasionally interfingers with the Toarcian-aged coarse-grained sandstones of the Tofte Formation that represent localised point-sourced prograding delta fans (Van Cappelle *et al.*, 2017). The upper boundary of the Båt Group and the contact to the overlying Fangst Group is defined at the boundary between muddy shelf deposits of the Ror Formation and the sandy deposits of the Ile Formation (Dalland *et al.*, 1988; Bunkholt *et al.*, 2025).

METHODS & DATASET

The dataset investigated in this study comprises extensive wireline log, core, and core

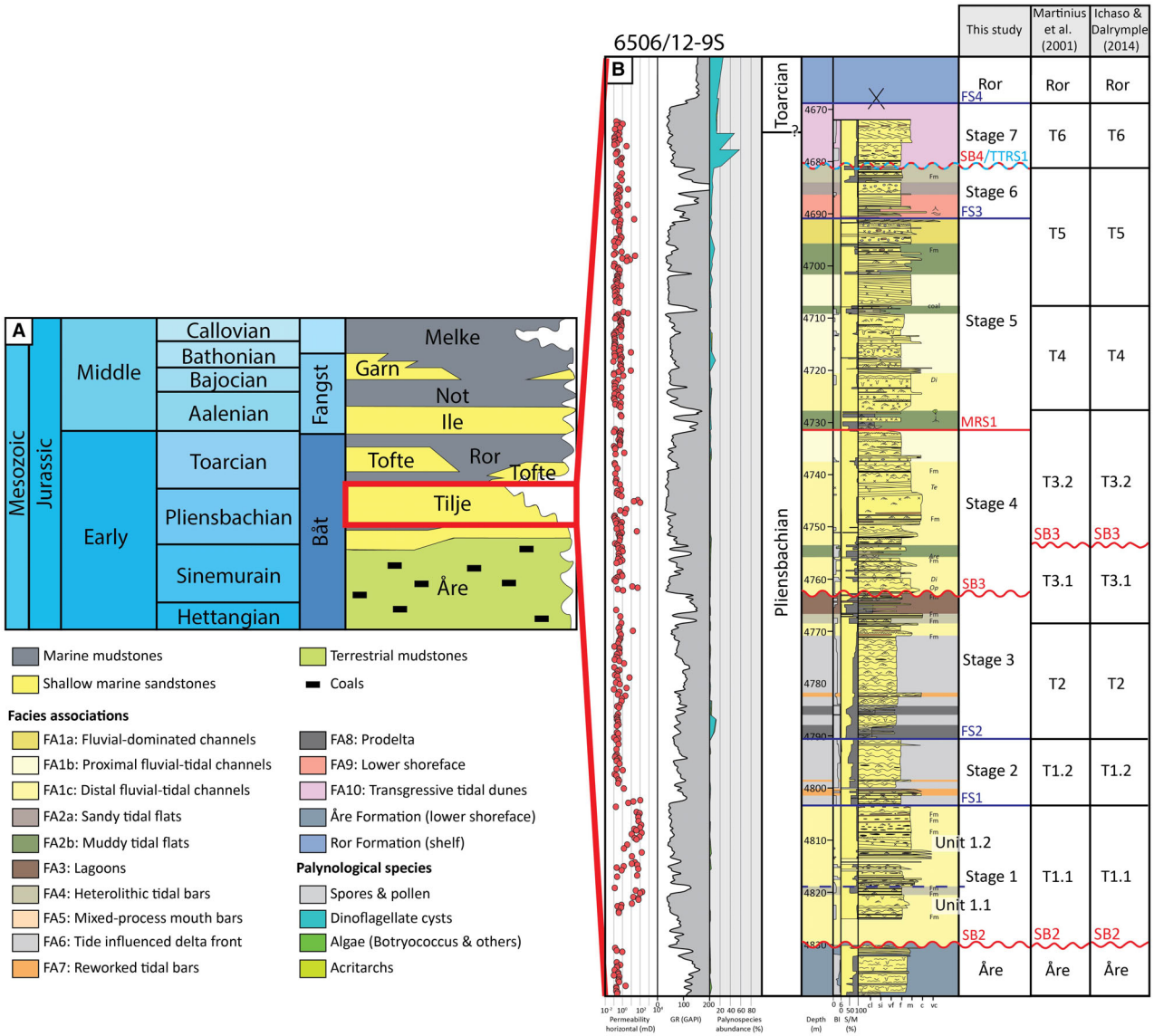

Fig. 2. (A) Lithostratigraphic chart of the Lower and Middle Jurassic units on the Halten Terrace. Modified after Bunkholt *et al.* (2025). The Tilje Formation is highlighted in the red box. (B) Sedimentological log of the Tilje Formation in the Smørbukk Field. Curves (from left to right): horizontal permeability (mD), gamma ray (GAPI), palynological species abundance, age, depth (MD), bioturbation index, sandstone/mudstone percentage, sedimentological log with facies associations coloured, stratigraphic scheme used in this study, stratigraphic scheme from Martinius *et al.* (2001) and stratigraphic scheme from Ichaso & Dalrymple (2014).

plug data from the Tilje Formation, in the Smørbukk Field and one 2D seismic line through the central Halten Terrace, available on the DISKOS database. A total of 690 m of core from four wells (6506/12-1, 6506/12-10, 6506/12-9S and 6506/11-2; Fig. 1) were logged at a scale of 1:25 for detailed sedimentological investigation, including descriptions of lithology, grain size, sorting, sedimentary structures and trace fossils. The bioturbation diversity and intensity were recorded using the seven-degree bioturbation index (BI) of Taylor & Goldring (1993). Biostratigraphic, bio and palynofacies data (Equinor in-house data) were integrated with the sedimentary facies data where available. Eight additional wells were

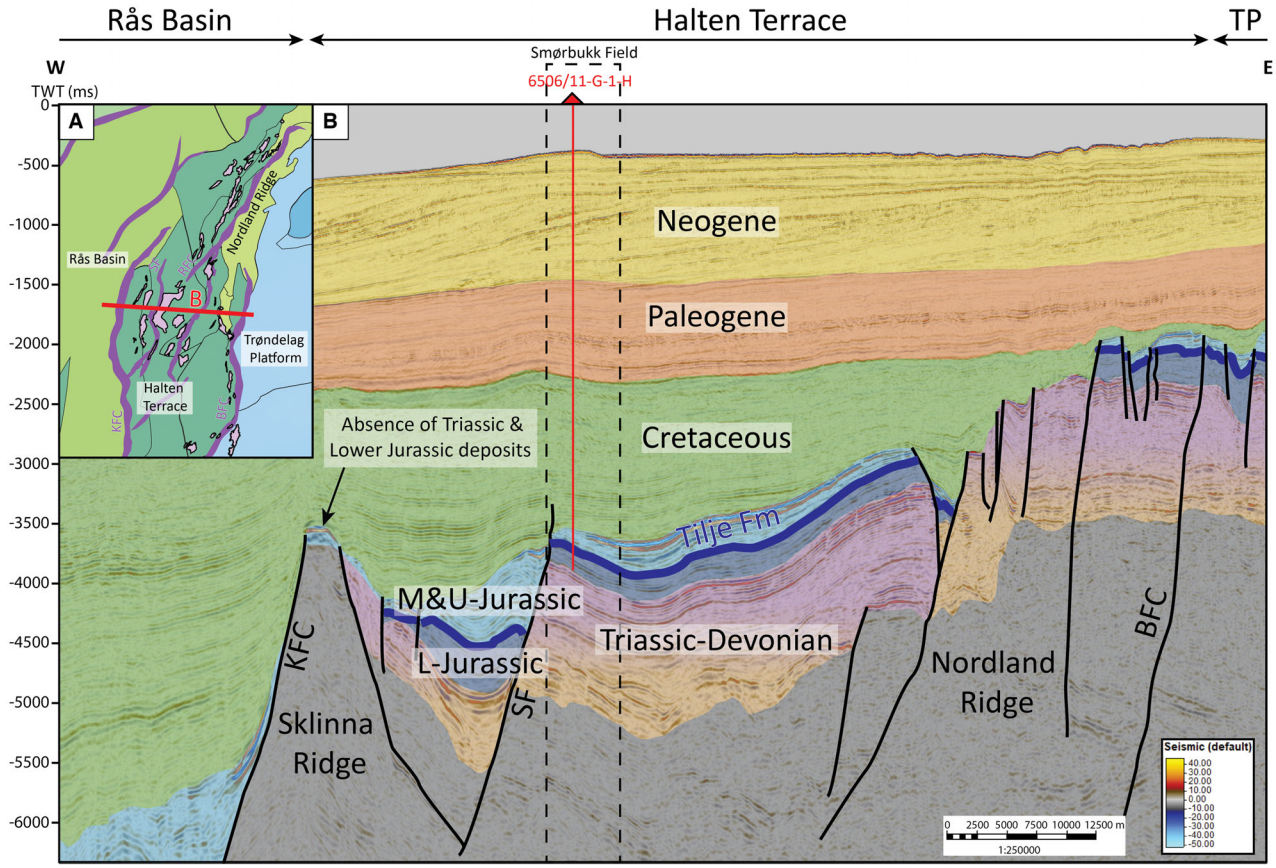

Fig. 3. (A) Location map showing the main structural elements of the study area, the principal faults and the fields (see Fig. 1 for legend). The position of the seismic line is shown by the red line. BFC, Bremstein Fault Complex; KFC, Klakk Fault Complex; RFC, Revfallet Fault Complex; SF, Smørbukk Fault; TP, Trøndelag Platform. (B) Interpreted seismic reflection line. The Smørbukk Field is highlighted by the black stippled lines. Well 6506/11-G-1-H (see Fig. 1C for locality and Fig. 6 for correlation) is highlighted by the red line. Note the absence of Lower Jurassic and Triassic deposits on the Sklinna ridge, indicating that this was an emergent basement high supplying sediments during deposition of the studied Tilje Formation.

investigated based on core photos and wireline log data (Fig. 1), identifying depositional environments based on the facies analysis developed in logged cores.

Petrophysical data were used in this study to investigate the stratigraphic and regional distribution of high-permeability intervals throughout the Tilje Formation in the Smørbukk Field. The petrophysical data were made available by TGS through the Facies Map Browser database. This includes wireline logs and porosity and permeability data from over 5000 core plug samples for all investigated wells. Permeability data were used to produce permeability maps for each stratigraphic interval of the Tilje Formation by averaging the permeability (geometric average) of sandstone bodies for the entire stratigraphic interval. Additionally, 550 core plug samples from two wells (see Fig. 1 for location) were used to investigate the relationships between permeability, facies and facies associations. Permeability values used throughout this study always refer to horizontal permeability. Permeability is referred to as *high* if it is above 50 mD, *medium* if it is between 1 and 50 mD and *low* if it is lower than 1 mD.

Petrographical data include 56 resin-impregnated thin sections made from samples collected from four wells (Fig. 1) and prepared for optical microscopy. Petrographic analysis was undertaken for compositional and textural analysis with a particular focus on the identification and characterisation of grain-coating and pore-filling chlorite.

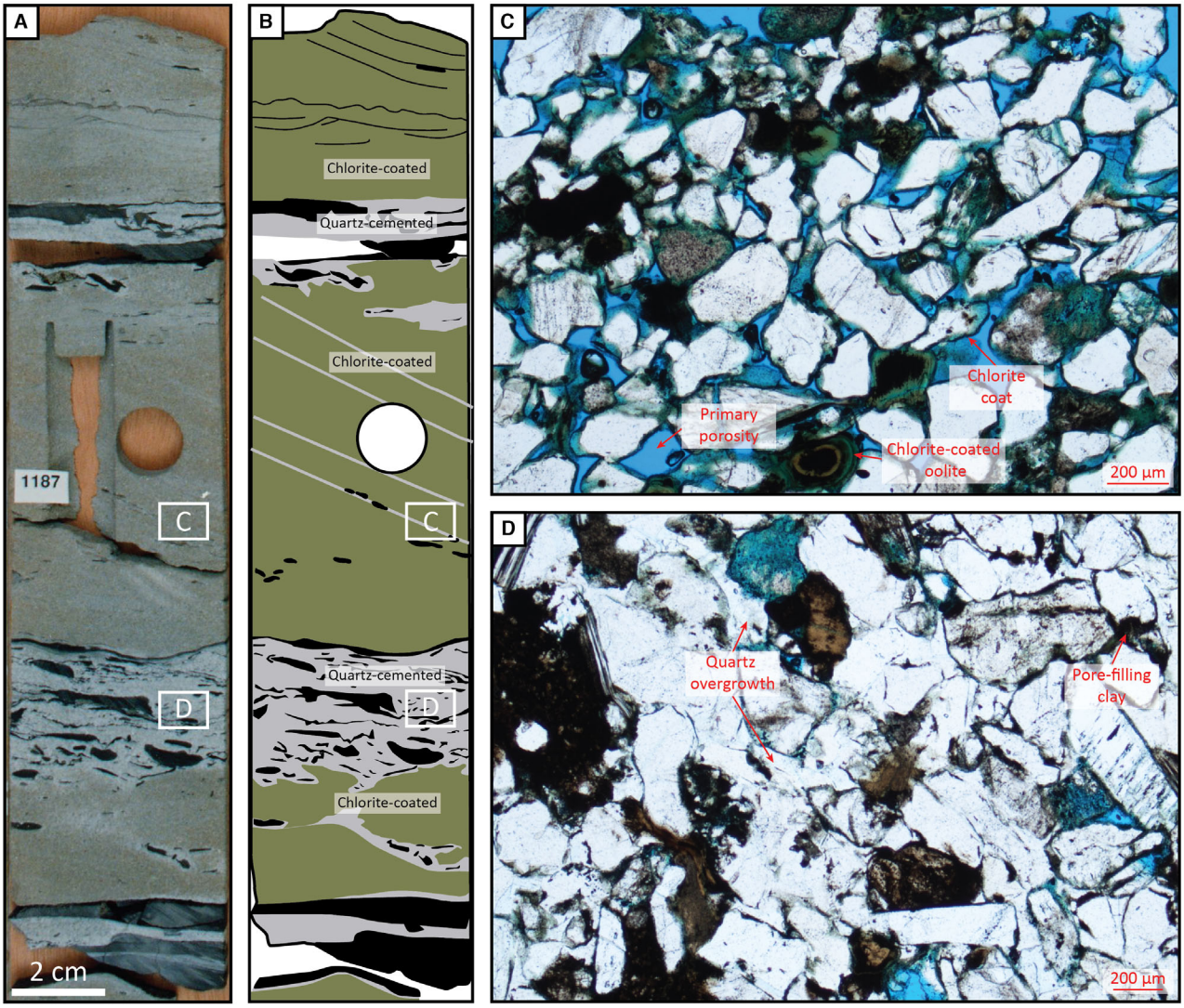

Fig. 4. (A, B) Details of core showing the small-scale changes between chlorite-coated (C) and quartz-cemented intervals (D).

RESULTS

Facies associations

This study presents a new sedimentological framework for the Tilje Formation in the Smørbukk Field, which will be further compared with previous studies (c.f., Martinius *et al.*, 2001; Ichaso & Dalrymple, 2014). A total of 23 sedimentary facies has been defined based on descriptions of lithology, grain size, sorting, sedimentary structures and trace fossils diversity and intensity. These are summarised in Table S1 and form the building block of the 10 facies associations recognised in the investigated core and wells (Figs 5 and 6 and Table 1). The interpreted depositional environments are fluvial-tidal channels (FA1), tidal flats (FA2), lagoons (FA3), heterolithic tidal mouth bars (FA4), mixed-process mouth bars (FA5), tide-influenced delta front (FA6), reworked tidal bars (FA7), prodelta (FA8), lower shoreface (FA9) and transgressive tidal dunes (FA10).

FA1: Fluvial-tidal channels

Description

Facies association 1 consists of erosive-based, fining-upwards sandstone bodies dominated by sandstone facies showing abundant cross-bedding (F4), current ripple cross-lamination

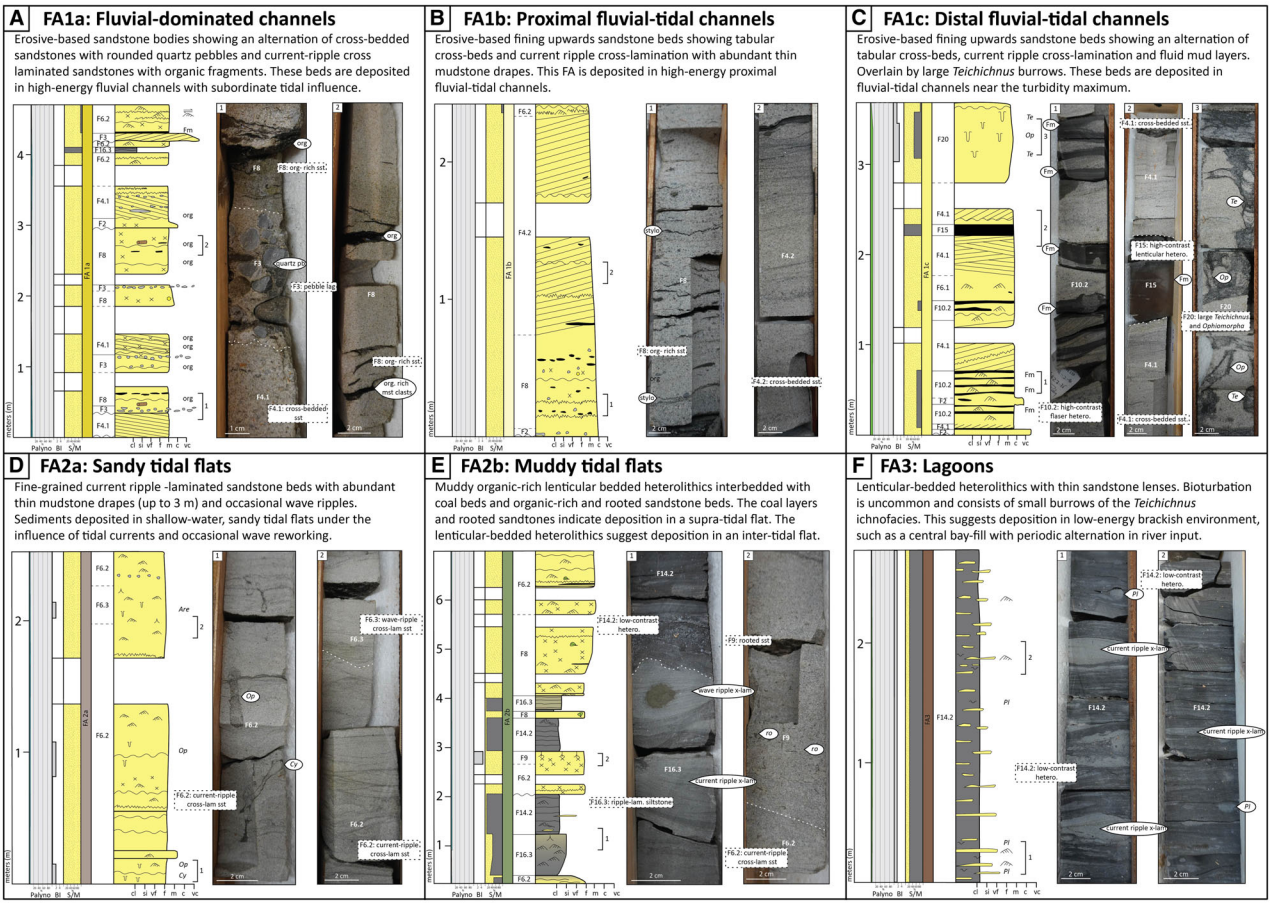

Fig. 5. Representative logs and detailed photos of the facies associations: (A) Fluvial-dominated channels (FA1a); (B) Proximal fluvial-tidal channels (FA1b); (C) Distal fluvial-tidal channels; (D) Sandy tidal flats (FA2a); (E) Muddy tidal flats (FA2b); (F) Lagoons (FA3); (G) Heterolithic tidal mouth bars (FA4); (H) Mixed-process mouth bars (FA5); (I) Tide-influenced delta-front (FA6); (J) Reworked tidal bars (FA7); (K) Prodelta (FA8); (L) Lower shoreface (FA9); (M) Transgressive tidal dunes (FA10). Palynospecies abundance (Palyno), bioturbation index (BI), sandstone/mudstone ratio, facies association and facies are displayed to the left of the logs. (N) Legend.

(F6) and high-contrast flaser-bedded heterolithics (F11). These sandstone bodies are commonly amalgamated to up to 20 m thick intervals. According to different internal facies variations, this facies association has been subdivided into: (i) FA1a with organic-rich sandstones (i.e., with abundant plant debris and fragments); (ii) FA1b dominated by cross-bedded and ripple cross-laminated sandstones showing common mudstone drapes; and (iii) FA1c with abundant fluid muds and elongated mudstone clasts interbedded with cross-bedded and ripple cross-laminated sandstones.

Interpretation

Facies association 1 is interpreted as channelised sandbodies based on its erosive-based, fining-upward trend and the abundance of high-energy tractional sedimentary structures. The abundance of mudstone drapes, fluid mud layers, mudstone clasts and bidirectional current ripples suggests deposition by tidal currents. Therefore, FA1 is interpreted as representing single or amalgamated fluvial-tidal channels. Differences in sedimentary structures, bioturbation and sand-mud ratio occur within this facies association and reflect subtle changes in depositional processes according to the relative influence of fluvial and tidal processes.

FA1a: Fluvial-dominated channels

Description.

Facies association 1a consists of erosive-based sandstone bodies occurring in bedsets up to 5 m

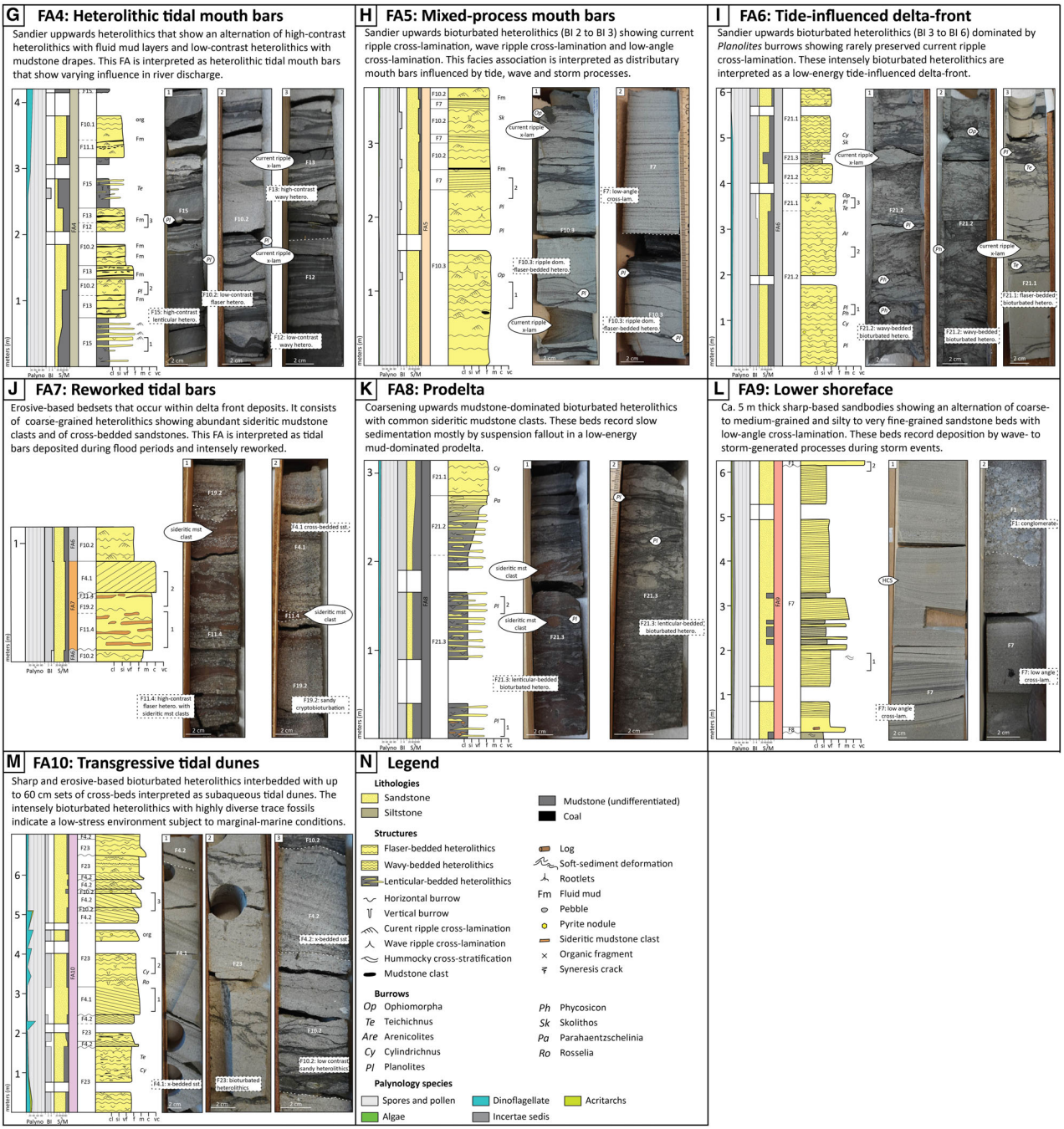

Fig. 5. (continued)

thick (Fig. 5A). It typically shows coarse- to medium-grained tabular cross-bedded sandstones (F4.1) alternating with bidirectional current ripple cross-laminated sandstones (F6.1) that show thin (<1 mm) mudstone drapes on the foresets of the ripples. These alternate with intervals of organic-rich sandstones (F8) showing thicker (up to 3 mm) organic-rich mudstone drapes, together with mudstone clasts, organic fragments (i.e., plant debris <1 cm) and pyrite nodules. Thick (>1 cm) homogeneous, massive mudstone layers occur occasionally. Additionally, there is a rhythmic occurrence of erosive-based pebble lags throughout this facies association, which occur within or at the base of cross-bedded intervals and show well-rounded quartzitic pebbles (up to

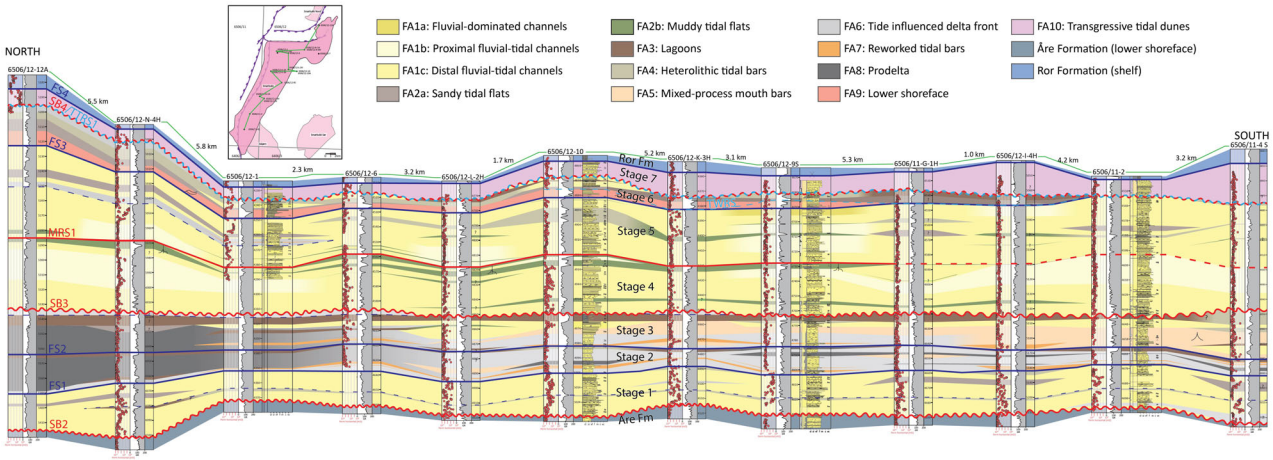

Fig. 6. North–south correlation panel across the Smørbukk Field. Each well is shown with (from left to right): permeability (mD), gamma ray (GAPI), depth (MD) and occasionally sedimentological log. See Figs 4 and 5 for core details. FS, major flooding surface; MRS, major regressive surface; SB, sequence boundary; SB–TTRS, sequence boundary–transgressive tidal ravinement surface; TWRS, transgressive wave ravinement surface.

3 cm diameter). This facies association is characterised by the absence of bioturbation (BI 0) and is dominated by pollens and spores.

Interpretation.
Facies association 1a is interpreted as fluvial-dominated channels showing subordinate tidal influence during river interflood periods. The erosive-based nature of the sandstone beds and the coarse grain size indicate deposition by high-energy erosive flows in channelised environments. The rhythmic alternation of cross-stratified beds with rounded pebbles and ripple cross-laminated beds is attributed to differences in river discharge. The pebbles were transported by high-energy flows during river floods and were associated with the formation of high-energy 3D subaqueous dunes. River discharge was likely too high to allow tidal reworking, leading to the deposition of coarse-grained fluvial-dominated intervals. The beds deposited during periods of lower fluvial discharge (interflood) show bidirectional current ripples and abundant mudstone drapes, indicating tidal reworking and deposition of finer-grained sediments during slack-water periods. The low-energy flows carried abundant light organic debris (Gugliotta *et al.*, 2016), resulting in the deposition of organic-rich drapes and fragments. The absence of bioturbation throughout this facies association suggests that strong fluvial discharge resulted in high sedimentation rates that prevented biogenic colonisation (Gingras & MacEachern, 2012). Facies association 1a shows the coarsest grains observed throughout the Tilje Formation, suggesting relatively proximal, high-energy channels.

FA1b: Proximal fluvial-tidal channels

Description.
Facies association 1b consists of up to 6 m thick erosive-based, fining-upward sandstone bedsets (Fig. 5B). The lower part of this FA typically consists of coarse- to medium-grained sandstone beds with abundant small-scale organic-rich mudstone clasts (up to 3 cm), organic fragments (i.e., plant debris) and occasionally a pebble lag. It is fining upwards into medium to fine-grained tabular cross-bedded sandstone with thin mudstone drapes and alternates with fine-grained bidirectional current ripple cross-laminated sandstone. The ripple cross-laminated facies show abundant thin mudstone drapes (single and double) typically on the foresets of ripples and thicker (up to 3 mm) drapes overlying the ripples. Many of these mudstone drapes are organic-rich and some show small pyrite nodules. Very rarely thicker fluid mud layers (>1 cm) also occur. This interval also shows abundant small-scale stylolites (ca. 5 per metre). Throughout this facies association bioturbation is absent to very rare (BI 0 to BI 1) and includes small-sized *Ophiomorpha* and *Teichichnus*. Facies association 1b is dominated by spores and pollen, and occasional *Botryococcus* and other algae (Fig. 5B).

Table 1. Key characteristics of the 10 facies associations observed throughout the Tilje Formation in the Smørbukk Field.

Facies association	Dominant lithology	Characteristic sedimentary structures	Bioturbation intensity and ichnofacies	Palynospecies diversity
FA1a: Fluvial-dominated channels	Sandstone with occasional mudstone clasts.	Tabular cross-bedding. Abundant rounded quartz pebbles and organic fragments.	BI 0.	Spores and pollens.
FA1b: Proximal fluvial-tidal channels	Sandstone with common mudstone clasts.	Tabular cross-bedding and current ripple cross-lamination. Common mudstone clasts and organic fragments.	BI 0 to BI 1.	Spores and pollens.
FA1c: Distal fluvial-tidal channels	Heterolithic sandstone with fluid mud layers and mudstone clasts.	Tabular cross-bedding and current ripple cross-lamination. Abundant fluid muds and mudstone clasts.	BI 0 to BI 6 towards the top. Low diversity *Skolithos* assemblage.	Spores and pollens, and occasional algae.
FA2a: Sandy tidal flats	Heterolithic sandstone with thin mudstone drapes.	Current ripple cross-lamination and occasional wave ripple cross-lamination.	BI 1 to BI 3.	Spores and pollens.
FA2b: Muddy tidal flats	Organic-rich siltstone and sandstone.	Organic-rich siltstones with current ripple cross-lamination and soft-sediment deformation. Rooted sandstone beds.	BI 0 to BI 3. *Psilonichnus*.	Spores and pollens.
FA3: Lagoons	Mudstone with lenticular sandstone beds.	Thin sandstone lenses with occasional current ripple cross-lamination.	BI 1 to BI 2. *Teichichnus*.	Spores and pollens, Botryococcus and other algae.
FA4: Heterolithic tidal mouth bars	Heterolithic sandstone with abundant fluid muds and mudstone drapes.	Abundant thick fluid mud layers and mudstone clasts. Current ripple cross-lamination.	BI 0 to BI 4. *Teichichnus*.	Spores and pollens, and dinoflagellate cysts.
FA5: Mixed-process mouth bars	Heterolithic sandstone with abundant mudstone drapes.	Current and wave ripple cross-lamination, and low-angle cross-lamination. Abundant thin mudstone drapes.	BI 1 to BI 3. *Rosselia*.	Spores and pollens.
FA6: Tide-influenced delta-front	Heterolithic sandstone with abundant mudstone drapes.	Abundant mudstone drapes. Bioturbated beds, sedimentary structures are rarely preserved.	BI 4 to BI 6. *Rosselia*.	Spores and pollens, and dinoflagellate cysts.

Table 1. (continued)

Facies association	Dominant lithology	Characteristic sedimentary structures	Bioturbation intensity and ichnofacies	Palynospecies diversity
FA7: Reworked tidal bars	Sandstone beds with abundant sideritic mudstone clasts.	Tabular cross-bedding and abundant sideritic mudstone clasts. Bioturbated beds, sedimentary structures are in places not preserved.	BI 5 to BI 6. Cryptobioturbation.	Spores and pollens.
FA8: Prodelta	Mudstone with lenticular sandstone beds.	Bioturbated beds, sedimentary structures are rarely preserved. Abundant sideritic mudstone clasts.	BI 3 to BI 6. *Cruziana* (restricted).	Spores and pollens, and dinoflagellate cysts.
FA9: Lower shoreface	Sandstone and occasional siltstone beds.	Low-angle cross-lamination and occasional wave ripples and hummocky cross-stratification.	BI 0.	Spores and pollens.
FA10: Transgressive tidal dunes	Sandstone with abundant mudstone drapes.	Alternation of tabular cross-bedding beds and bioturbated beds. Occasional mudstone drapes.	BI 2 to BI 4. *Cruziana* (diverse).	Spores and pollens, and dinoflagellate cysts.

Interpretation.
Facies association 1b is interpreted as being fluvial-dominated, tide-influenced and deposited in relatively proximal settings within the tidal limit. This is supported by the presence of pollen, spores and algae, which suggest freshwater influx in relatively proximal settings. Facies association 1b includes channelised sandbodies with erosive bases and a fining upwards trend. The basal erosive beds with mudstone clasts and occasional pebble lags were deposited by high-energy, highly erosive flows and represent channel lags. The tabular cross-bedded sandstone beds were deposited by unidirectional flows due to the migration of 3D subaqueous dunes on the channel base. As the flow decelerated, finer-grained current ripple cross-laminated sandstones were deposited. The bidirectionality of the current ripples and the abundance of thin mudstone drapes suggest frequent reworking by tidal currents. Throughout FA1b, sedimentation rates were too high for consistent biogenic colonisation (Gingras & MacEachern, 2012).

FA1c: Distal fluvial-tidal channels

Description.
Facies association 1c typically shows an upward fining trend from a thin, erosive-based basal coarse-grained sandstone lag (F2) to dominantly current ripple cross-laminated sandstones (F6.1) and tabular- cross-bedded sandstone beds (F4.1). The ripple cross-laminated sandstones show bidirectional current ripple cross-lamination and thin (<1 cm) mudstone drapes (single and double). They are occasionally interbedded with coarse to fine-grained bed sets up to 80 cm that show tabular cross-beds and mudstone drapes (Fig. 5C). These can be distinguished from the classical cross-bedded sets because they show (i) a high concentration of mudstone drapes at the bottomset of the cross-bed set; (ii) a rhythmic alternation in grain size between the coarse-to-medium-grained cross-beds and the finer-grained material deposited on the foresets of these cross-beds; and (iii) steepening-upwards cross-bed foresets. Facies association 1c is also characterised by the abundance of thick (from 1 cm up

to 10 cm) homogeneous mudstone layers (i.e., fluid mud layers) and rounded mudstone clasts, both of which are often sideritic. The uppermost part of this facies association typically consists of bioturbated sandstone beds (BI 4 to BI 6) showing quasi-exclusively large (>5 cm in height) *Teichichnus* and *Diplocraterion* burrows (F20) and uncommon *Ophiomorpha*, and *Arenicolites* burrows. The biogenic traces appear to mainly rework fluid mud layers, often resulting in a muddy bioturbated texture (F19.1). This facies association is dominated by spores and pollens, but also shows local fluctuations in the abundance of *Botryococcus*, and other algae (Fig. 5C).

Interpretation.
Facies association 1c is interpreted as representing fluvial-tidal channels deposited in relatively distal locations, in proximity to the tidal maximum. This facies association shows sets of cross-beds interpreted as subaqueous tidal dunes showing evidence of tidal bundling (Boersma, 1969). The finer-grained material was deposited during slack-water periods between successive tidal cycles. The higher concentration of mudstone drapes at the bottomset is deposited around neap tide when the flow velocities are lower, and dune height decreases (Dalrymple & Rhodes, 1995). In contrast with FA1a and FA1b, a high proportion of the mud in this facies association is deposited as thick fluid mud layers rather than as thin mudstone drapes. This suggests that the concentration of mud was sufficiently high to form a high-density basal fluid mud layer (Ichaso & Dalrymple, 2009; MacKay & Dalrymple, 2011). This occurs in proximity to the tidal maximum, where the mixing of fresh and saltwater results in high mud flocculation (Van den Berg *et al.*, 2007; MacKay & Dalrymple, 2011). This facies association is characterised by a quasi-monospecific trace fossil suite showing opportunistic colonisation towards the top of the channels during periods of lower sedimentation rates (Gingras & MacEachern, 2012). Additional trace fossils are restricted to *Ophiomorpha* and *Arenicolites*, characteristic of a *Teichichnus* ichnofacies assemblage (Gingras *et al.*, 2025), suggesting stressed brackish conditions. The occasional presence of *Botryococcus* and other algae indicates fluctuating freshwater influx or brackish influence (Guy-Ohlson, 1992).

FA2: Tidal flats

FA2a: Sandy tidal flats

Description.
Facies association 2a consists mainly of fine-grained current ripple-laminated sandstone to siltstone beds that show abundant thin mudstone drapes (F6.2; Fig. 5D). Occasional wave ripples and wave-reworked current ripples occur (F6.3). This facies association is low to moderately bioturbated (BI 1 to BI 3) and shows *Ophiomorpha*, *Cylindrichnus* and *Arenicolites*. Occasionally, subrounded quartzitic pebbles occur in lags towards the top of this facies association.

Interpretation.
Facies association 2a is interpreted to have been deposited in the subtidal to lower intertidal area, as indicated by the lack of evidence for subaerial exposure (i.e., rootlets and coal beds). The dominant influence of tidal currents is supported by the occurrence of bidirectional current ripples and the abundant thin mudstone drapes (single and double), which suggest deposition by suspension fall-out during slack-water periods. This facies association also shows evidence of reworking by wave processes. Therefore, FA2a was likely deposited in shallow-water tidal flats under the action of tidal currents and occasionally reworked by wave action.

FA2b: Muddy tidal flats

Description.
This facies association consists of organic-rich mudstone beds interbedded with thin sandstone lenses (lenticular-bedded heterolithics), coal beds and sandstone beds that show abundant organic fragments and/or rootlets (Fig. 5E). The lenticular-bedded heterolithics (F14.2) show soft-sediment deformation structures in the muddy beds. The very fine-grained sandstone lenses are thin (up to 2 cm thick) and commonly show small current ripple cross-lamination and occasional wave ripple lamination. Coal beds (up to 10 cm thick) occasionally overlay these lenticular-bedded heterolithics. The sandstone beds contain abundant organic fragments and very thin coal layers (<1 cm) as well as a few organic-rich mudstone drapes and common stylolites. They are occasionally disturbed by abundant root traces. Bioturbation (BI 0 to BI 3) occurs mostly in the muddy and silty beds and consists of root traces and occasionally of small-scale *Teichichnus* and *Skolithos*.

Interpretation.
Facies association 2b was deposited in intertidal flats that were inundated during high tides and reworked by tidal and wave processes during storm events. The presence of coal layers and rooted intervals suggests periods of subaerial exposure and soil formation. This facies association was thus deposited in a vegetated subaerial delta plain area (i.e., tidal marsh), where sandy intervals accumulated during occasional flooding. The small-scale ripples reflect deposition during river floods and minor wave reworking.

FA3: Lagoons

Description
Facies association 3 consists of lenticular-bedded heterolithics (F14.2) with a low sandstone percentage (up to 30%). The very fine- to fine-grained sandstone lenses are thin (up to 3 cm) and occasionally preserve current ripple cross-lamination (Fig. 5F). Thicker medium- to coarse-grained sandstone lenses occur occasionally. This facies association is weakly bioturbated (BI 1 to BI 2) with small *Planolites* and *Teichichnus*. It also shows an increase in the abundance of *Botryococcus* and other algae.

Interpretation
Facies Association 3 represents sedimentation in a protected low-energy environment, such as a central bay-fill or lagoonal-fill, where deposition occurred mainly as suspension fall-out. The restricted diversity of trace fossils, together with the small size of the burrows of the *Teichichnus* ichnofacies (Gingras *et al.*, 2025), suggests stressed brackish settings. The thin sandstone lenses suggest periodic river input transporting fine-grained sands into the protected muddy lagoons. The cyclic variation in the number, thickness and grain size of these sandy intervals could indicate flood-interflood periods. This is also supported by the presence of *Botryococcus* and other algae characteristic of freshwater environments (Guy-Ohlson, 1992).

FA4: Heterolithic tidal mouth bars

Description
Facies association 4 consists of heterolithic deposits that are coarsening upward from mudstone-dominated heterolithics towards the base to sandstone-dominated heterolithics towards the top (Fig. 5G). The sandstone beds are very fine- to medium-grained and typically show bidirectional current ripple cross-lamination. This facies association is characterised by its highly heterolithic nature, showing abundant thick fluid mud layers and thin mudstone drapes. Additionally, FA4 shows a rhythmic alternation between high-contrast (i.e., heterolithics dominated by thick fluid mud layers) and low-contrast heterolithics (i.e., heterolithics dominated by thin mudstone drapes). The high-contrast heteroliths commonly show fine- to medium-grained sandstone layers (up to 10 cm thick) with occasional current ripple cross-lamination and occasional *Planolites*, and *Teichichnus* burrows (BI 0 to 2). The fluid mud layers are thick and homogeneous (up to 15 cm thick) and occasionally show syneresis cracks. The low-contrast heterolithics are dominated by fine- to very fine-grained sandstone, showing current ripple cross-lamination and abundant thin mudstone drapes. Bioturbation is moderate to common (BI 3 to BI 4) and consists mostly of *Planolites* and *Teichichnus* burrows, although rare *Ophiomorpha* occur. This facies association is occasionally capped by a ca. 1 m thick erosive-based fine- to medium-grained sandstone bed that shows tabular cross-bedding and bidirectional current ripple cross-lamination.

Interpretation
Facies association 4 is interpreted as heterolithic tidal mouth bar deposits that show varying influence of river discharge during flood and interflood periods. It is occasionally capped by erosive-based sandstone beds interpreted as terminal distributary channel fills. The abundance of thick homogeneous fluid mud layers in this facies association suggests deposition by tidal currents able to suspend sufficient mud to form fluid mud layers (Ichaso & Dalrymple, 2009; MacKay & Dalrymple, 2011). This occurs in proximity to the turbidity maximum (Van den Berg *et al.*, 2007; MacKay & Dalrymple, 2011). FA4 commonly shows an alternation between two types of heterolithics (i.e., high- and low-contrast), reflecting differences in river discharge. The high-contrast heterolithics suggest deposition during river flood periods when coarser sediments are transported by the river and the turbidity maximum is displaced seaward, leading to high concentration rates of mud and deposition of fluid mud layers at the mouth bars (Dalrymple *et al.*, 2015; Gugliotta *et al.*, 2016). The low-contrast heterolithics are deposited during interflood periods when mud is mainly deposited as thin drapes on the mouth bars during slack-water

periods. Similarly, the bioturbation index varies cyclically throughout this facies association, with the low-contrast heterolithics showing a higher bioturbation index (BI 3 to 4) than the high-contrast heterolithics (BI 0 to 2). The low-diversity trace fossil assemblage of the *Teichichnus* ichnofacies (Gingras *et al.*, 2025) suggests stressed brackish conditions.

FA5: Mixed-process mouth bars

Description

This facies association consists of up to ca. 5 m thick intervals of fine- to very fine-grained sandstone-dominated heterolithics (Fig. 5H). It is dominated by bioturbated heterolithics, which typically show a cyclic variation in bioturbation intensity and diversity, with mudstone beds typically being sparsely bioturbated (BI 1 to BI 2) and showing mainly *Planolites* and occasional *Teichichnus*. Sandstone beds are sparsely to moderately bioturbated (BI 1 to BI 3), showing *Teichichnus*, *Ophiomorpha*, *Skolithos*, *Phycosiphon* and *Siphonicnus*. The preserved sedimentary structures consist of abundant bidirectional current ripples, wave ripples and low-angle cross-lamination. They show abundant thin (up to 3 mm) mudstone drapes (single and double), and thicker (>1 cm) homogeneous fluid mud layers also occur.

Interpretation

Facies association 5 represents distributary mouth bars showing a mixed influence of fluvial, tidal, wave and storm processes. The dominated flaser-bedded heterolithics with abundant mudstone drapes in FA5 suggest deposition by tidal currents during slack-water periods. The wave ripple and low-angle cross-laminated intervals suggest occasional deposition by oscillatory or combined flows and are interpreted as representing tempestite deposits (Arnott & Southard, 1990). The cyclic alternation in bioturbation diversity and intensity reflects episodic deposition and frequent shifts in dominant depositional processes (MacEachern & Bann, 2020, 2023).

FA6: Tide-influenced delta front

Description

Facies association 6 typically consists of sandier upwards wavy-bedded and flaser-bedded heterolithics (F10.1 and F10.2; Fig. 5I). It is typically moderately to intensely bioturbated (BI 4 to BI 6) and is dominated by *Planolites*, *Teichichnus* and occasional *Paleophycus*, *Cylindrichnus*, *Phycosiphon*, *Rhizocorallium*, *Ophiomorpha*, *Siphonicnus*, *Rosselia* and *Artichnus*. These bioturbated beds show abundant thin and continuous single to double mudstone drapes. Primary sedimentary structures are typically not preserved due to the high bioturbation index, but in places, less bioturbated ripple cross-laminated heterolithic intervals occur, together with rare wave ripples (Fig. 5I). This facies association occasionally shows a peak in the relative abundance of dinoflagellate cysts (Fig. 5I).

Interpretation

Facies association 6 is interpreted as a low-energy, tidal-influenced delta-front prograding in shallow water. The dominance of low-diversity ichnogera in the highly bioturbated heterolithics of FA6 suggests deposition mainly in a stressed-environment subject to brackish conditions with reduced salinity. Some intervals, however, show a more diverse trace fossil assemblage with marine species (e.g., *Phycosiphon* and *Rosselia*). This suggests intermittent flooding events subject to fully marine conditions, also indicated by the occasional increase in dinoflagellate cysts. Throughout FA6, abundant mudstone drapes indicate deposition by tidal processes during slack-water periods. The occasional ripple cross-laminated intervals suggest deposition by bidirectional tidal currents, mostly, and occasional wave ripples indicate subordinate reworking by wave action.

FA7: Reworked tidal bars

Description

Facies association 7 occurs within the tide-dominated delta front deposits (FA6). It consists of sharp- and erosive-based coarse- to medium-grained bed sets up to 1.5 m thick (Fig. 5J). Typically, it is dominated by flaser-bedded heterolithics showing abundant sideritic fluid mud layers and large (>5 cm) sideritic mudstone clasts. Alternatively, it shows occasional thin (<1 mm) mudstone drapes. This facies association often transitions upward into coarse-grained tabular cross-bedded sandstone with occasional sideritic mudstone clasts. This facies association is intensely bioturbated (BI 5 to 6) and shows cryptobioturbation where individual burrows are rarely recognisable (Pemberton & Gingras, 2005; Pemberton *et al.*, 2008).

Interpretation

Facies association 7 represents reworked tidal bars prograding on the delta front. This facies association is distinguished from delta-front

deposits (FA6) by its coarse grain size, cryptobioturbation and the abundance of sideritic mudstone clasts, which suggest deposition by high-energy flows. The tabular cross-bedded intervals indicate deposition by unidirectional flows due to the migration of 3D subaqueous dunes. Low sedimentation rates allowed complete bioturbation.

FA8: Prodelta

Description

Facies association 8 consists of mudstone-dominated heterolithics that commonly show a high degree of bioturbation (BI 3 to BI 6) and a peak in the relative abundance of dinoflagellate cysts (Fig. 5K). It typically coarsens upwards from mudstone-dominated heterolithics with thin (<2 cm) sandstone lenses at the base to mixed sandstone-mudstone heterolithics and eventually sandstone-dominated heterolithics towards the top (Fig. 5K). Common sideritic mudstone clasts or siderite-cemented intervals typically occur towards the base of FA8 (Fig. 5K). Sedimentary structures are rarely preserved because of the high bioturbation index, albeit a few ripple cross-laminated heterolithic beds occur towards the top of this facies association. The bioturbated beds are dominated by *Planolites* burrows and also exhibit *Cylindrichnus*, *Siphonicnus*, *Teichichnus* and *Skolithos*.

Interpretation

Facies association 8 is interpreted as a low-energy tide-dominated prodelta possibly in a protected marine embayment. The bioturbated mudstone-dominated heterolithics with sideritic mudstone clasts suggest deposition in low-energy settings with slow sedimentation rates and biogenic reworking. The rarely preserved tractional structures suggest that the sandstone lenses are deposited by bidirectional currents, possibly during flood events. The restricted trace fossil assemblage of the *Cruziana* ichnofacies (MacEachern *et al.*, 2010) suggests a stressed environment.

FA9: Lower shoreface

Description

Facies association 9 consists of ca. 5 m thick sharp-based sandbodies, with an alternation of coarse- to medium-grained sandstone beds and silty to very fine-grained sandstone beds with low-angle cross-lamination (Fig. 5L). Occasional hummocky cross-stratification (HCS) and wave ripple cross-lamination occur in the silty to very fine-grained sandstone intervals. The coarser sandstone beds commonly show inclined plane-parallel cross-stratification and occasional organic-rich fragments. This facies association is occasionally capped by a thin (up to 15 cm) conglomerate lag that shows plane-parallel cross-lamination.

Interpretation

Facies association 9 represents lower shoreface deposits where deposition is mainly driven by wave-to-storm-generated processes. The low-angle cross-laminated siltstone to sandstone beds with local HCS are interpreted as tempestite event beds deposited below the fairweather wave base and above the storm wave base. The HCS record deposition by combined flows with high aggradation rates (Dumas & Arnott, 2006). The low-angle cross-laminated sandstone to siltstone beds indicate deposition under flow conditions corresponding to upper plane beds generated by combined flows (Arnott & Southard, 1990). These beds have been described from tempestite sequences elsewhere (Nøttvedt & Kreisa, 1987; Myrow, 1992; Midtgaard, 1996) and are part of a continuum of sedimentary structures generated during storm events under the influence of combined flows with varying influence of unidirectional flows.

FA10: Transgressive tidal dunes

Description

Facies association 10 occurs in the uppermost part of the Tilje Formation (Fig. 6). It consists mainly of sharp- and erosive-based interbedded bioturbated sandy heterolithics (F21.1, F22.1 and F19.1 towards the top) and cross-bedded sandstones (F4.1), low-contrast flaser-bedded heterolithics (F10.1 and F10.2) and subordinate organic-rich sandstones (F8). The bioturbated heterolithics dominate the lower part of FA10 and are progressively interbedded with cross-bedded and/or organic-rich sandstones upward (Fig. 5M). The cross-bedded sandstones are typically medium-grained and well-sorted and occur in beds up to 60 cm thick. They commonly exhibit a rhythmic grain size alternation between medium- and fine-grained sandstone and occasionally show a steepening upward trend of the foresets. Mudstone drapes and mudstone clasts (a few millimetres in diameter) are typically abundant at the bottomset of the cross-beds and then become sparser upwards. Additionally, sparse tabular sandy heterolithic beds (F10.1 and F10.2) exhibit current ripple cross-lamination with mudstone drapes and are likely to represent bottomsets. Thicker fluid mud

layers are occasionally present. Overall, all facies are moderately bioturbated (BI 2 to 4) and few beds are intensely bioturbated (BI 4 to BI 5). They exhibit a wide diversity of trace fossils including *Cylindrichnus*, *Asterosoma*, *Ophiomorpha*, *Teichichnus*, *Planolites*, *Rosselia*, *Arenicolites*, *Phycosiphon* and *Parahaentzschelinia*? The top metre of this facies association becomes progressively muddier upwards until it is overlain by the muddy heterolithics of the Ror Formation. It also shows a significant increase in the relative abundance of dinoflagellate cysts (up to 45%; Fig. 5M), that increase further in the overlying Ror Formation (Fig. 2).

Interpretation

Facies association 10 is interpreted as representing transgressive marine dunes deposited in open-marine settings. It is distinguished from the previous facies associations by the occurrence of intensely bioturbated heterolithics showing a diverse trace fossil assemblage of the *Cruziana* ichnofacies (MacEachern *et al.*, 2010). The high diversity of biogenic traces, together with the abundance of dinoflagellate cysts, indicates a low-stress environment subject to normal-marine conditions (c.f. MacEachern *et al.*, 2007). The cross-bedded sandstone beds are interpreted as subaqueous tidal dunes deposited by strongly asymmetric tidal currents. The grain size segregation observed in the foresets of the dune is commonly observed in tidal dunes, is likely related to pre-sorting of sediments by small superimposed bedforms (Reesink & Bridge, 2007, 2009; Reynaud & Dalrymple, 2012). Mudstone drapes that are concentrated at the bottomset of the dunes indicate repeated slack-water periods and are linked with periods of suppressed dune migration during periods of lower energy that allow flocculation of finer grain sizes. Similar cross-bedded tidal dunes have been observed from shallow-marine environments subject to strong tide influence elsewhere (c.f. Dalrymple & Rhodes, 1995, Olariu *et al.*, 2012). The rare fluid muds suggest transport from the river mouths, where mud concentration was high enough to form fluid mud layers (Nishida *et al.*, 2013). These fluid mud layers are likely to be further transported in more distal locations during transgression (Osman *et al.*, 2024). Intensely bioturbated heterolithic beds are deposited during periods of ceased dune migration, allowing low sedimentation rates and high reworking or are in a distal or adjacent location to the main tidal dunes (Olariu *et al.*, 2012).

Stratigraphic evolution

Eight regionally recognisable and relevant stratigraphic surfaces have been defined in the Smørbukk Field based on major shifts in depositional facies. These include three sequence boundaries (SB2, SB3 and one composite sequence boundary–transgressive tidal ravinement surface: SB4–TTRS1), four flooding surfaces (FS1, FS2, FS3 and FS4) and one maximum regressive surface (MRS1; Figs 2, 6 to 9). These stratigraphic surfaces were used as basis to divide the Tilje Formation in the Smørbukk Field into seven stratigraphic stages based on stacking patterns of facies associations. SB2 marks the base of the Tilje Formation and of Stage 1, FS1 marks the abrupt flooding of Stage 1, FS2 marks the abrupt flooding of Stage 2, SB3 marks the incision at the top of Stage 3, MRS1 marks the maximum regression at the top of Stage 4, FS3 marks the flooding at the top of Stage 5, SB4–TTRS1 marks the erosive top and the flooding of Stage 6 and FS4 marks the top of Stage 7 and the top of the Tilje Formation (Figs 2, 6, 8 and 9).

The base of the Tilje Formation (SB2) is characterised by a significant hiatus recording a major shallowing event indicated by the presence of fluvial-tidal channels of Stage 1 erosively overlying lower shoreface deposits of the Åre Formation (Figs 6 and 8). This basal incision surface (SB2) has also been picked as a major sequence boundary in previous studies (Martinius *et al.*, 2001; Ichaso & Dalrymple, 2014; Ichaso *et al.*, 2016) because it records a change in provenance age indicated by Sm/Nd isotopic data (Martinius *et al.*, 2001). Above SB2, sandy deposits of Stage 1 consist of a ca. 30 m thick interval of amalgamated fluvial-tidal channels (FA1c). A significant hiatus is recorded by FS1 which marks the abrupt flooding of the channelised deposits of Stage 1 by bioturbated heterolithic delta-front deposits of Stage 2 or prodelta deposits towards the north of the field (Fig. 7). Locally sandy bioturbated intervals interpreted as prograding tidal bars occur within Stage 2 (Fig. 6). These delta-front deposits of Stage 2 are abruptly flooded by the prodelta deposits of Stage 3 (FS2). Stage 3 consists of prograding prodelta, delta-front, mouth bar and fluvial-tidal channel deposits, overlain by a ca. 5 m thick mud-dominated interval interpreted as lagoonal or bay-fill deposits (Fig. 6). Locally in the north of the field, the lagoonal deposits are overlain by tide-influenced delta-front deposits, indicating a third major flooding episode that cannot

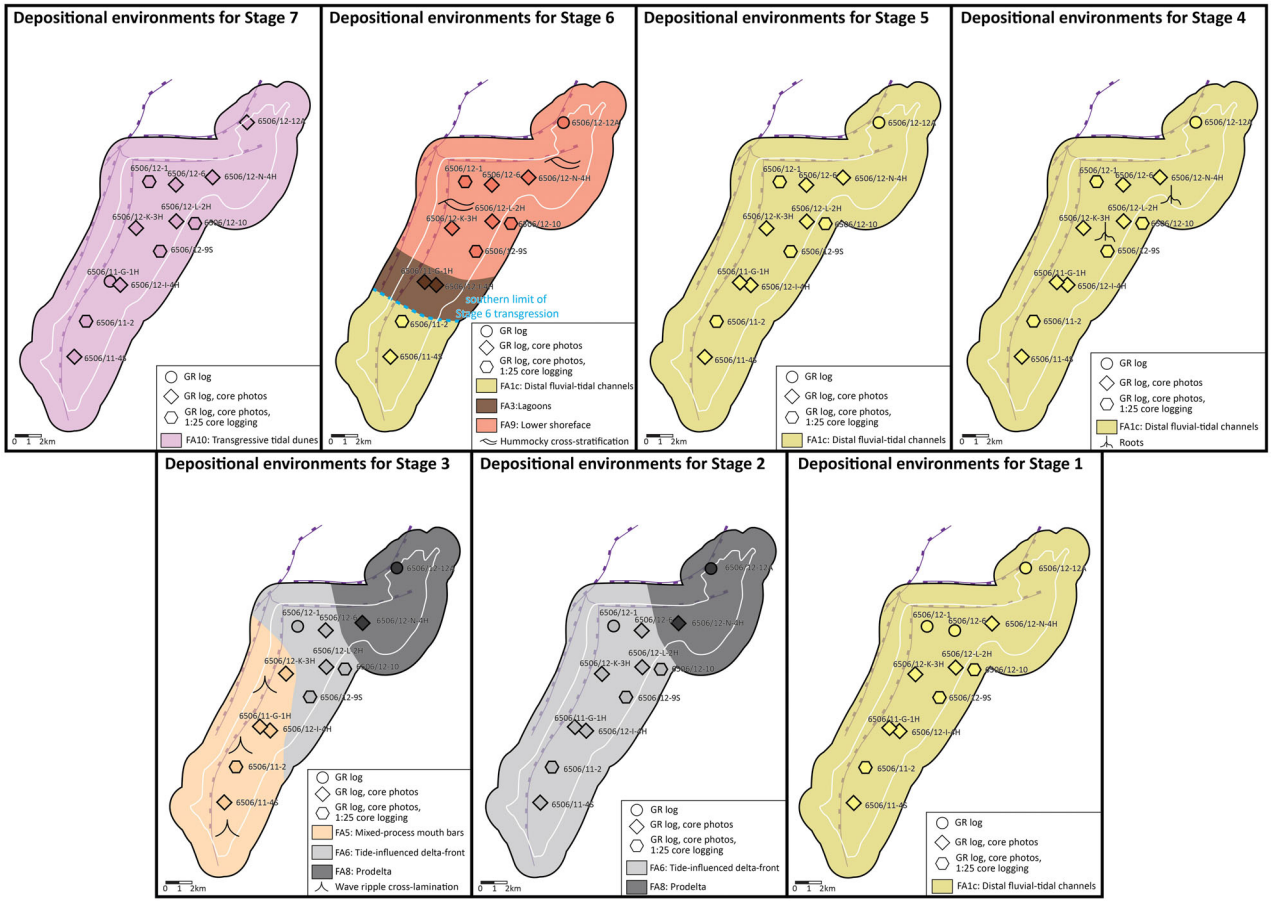

Fig. 7. Dominant depositional environments in the Smørbukk Field for each stratigraphic Stage. Well symbols highlight the type of data available. The outline of the Smørbukk Field is shown by a white line.

be correlated throughout the field (Figs 6 to 8). Stages 1 to 3 are thus part of the first sequence of the Tilje Formation which records the aggradation of fluvial-tidal channels and 2 major flooding episodes (FS1 and FS2) followed by the progradation of the tide-influenced delta (Fig. 8).

The abrupt transition from muddy lagoonal deposits or bioturbated delta front deposits of Stage 3 to amalgamated sandy deposits of Stage 4 is recorded by the erosive surface SB3 (Martinius *et al.*, 2001). Martinius *et al.* (2001) suggested that a major change in provenance age occurred few metres below SB3, being recorded by an Nd/Nd isotopic marker. The base of Stage 4 is therefore picked as a sequence boundary (SB3) as it likely records a major depositional hiatus. Stage 4 consists of an up to 45 m thick interval of amalgamated fluvial-tidal channels showing abundant plant fragments. It is capped by an organic-rich mudstone interval with thin coal layers and occasional sandstone beds showing root traces which record the maximum regression of the Tilje system (MRS1; Figs 6, 8 and 9). Above this surface, Stage 5 consists of another ca. 40 m thick interval of fluvial tidal channel and channel margin deposits (Figs 6 and 7). A third flooding event (FS3) records the abrupt flooding of the channelised deposits of Stage 5 by fine-grained sandy to silty lower shoreface deposits of Stage 6 (Figs 6 and 8). This surface records a major shift in dominant depositional processes from tide-dominated below to wave- and storm-dominated above, indicating the rapid transgression of the Tilje deltaic system (Fig. 8). Stages 4 to 6 are part of the second sequence of the Tilje Formation, which records the deposition of aggrading and prograding fluvial-tidal channels and the onset of the transgression of the Tilje system. The erosive contact between Stage 6 deposits and tidal dune deposits of Stage 7 records both field-wide incision and the onset of a transgressive cycle and

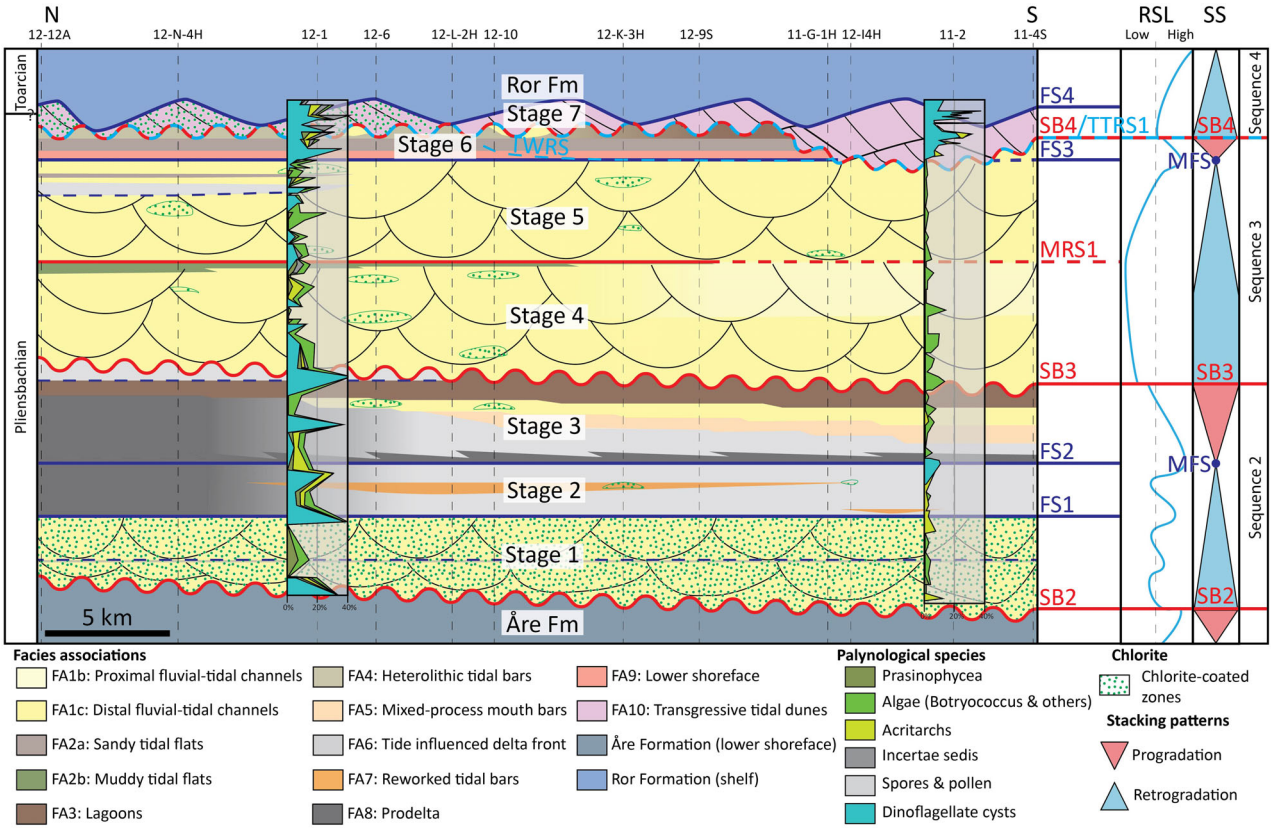

Fig. 8. Simplified stratigraphic section across the Smørbukk Field. Facies associations, architectural elements and chlorite-coated zones are simplified from Fig. 6. Stippled black lines show well locations. Palynological data (species abundance) from two wells is shown up to 40% for simplification. The remaining 60% consists of pollen and spores (light grey). RSL, relative sea level; SS, sequence stratigraphy.

is therefore picked as a candidate composite sequence boundary and transgressive surface of intra-latest Pliensbachian age (SB4–TTRS1; Figs 6, 8 and 9). A candidate fourth sequence is therefore proposed for the uppermost Tilje Formation (Stage 7), recording relative base sea-level fall and the onset of a transgressive cycle (Fig. 8). Further flooding is recorded by FS4 which marks the transition to the muddy early Toarcian-aged shelf deposits of the Ror Formation (Figs 2, 6 and 8).

Depositional model

The Tilje Formation is characterised by the highly heterolithic nature of most of the facies, showing abundant mudstone drapes and thick fluid mud layers preserved throughout most of the succession. Therefore, a depositional model of the Tilje Formation in the Smørbukk Field must reflect the substantial amounts of fine-grained material available for transport and deposition and that this fine-grained material remained mostly trapped in the basin. The depositional evolution of the Tilje Formation in the Smørbukk Field can be divided into two main phases, with Stages 1 to 5 representing deposition in a large tide-dominated embayment and Stages 6 to 7 representing deposition in a tide-influenced seaway.

Stages 1 to 5: Deposition of a large tide-dominated delta in a structural embayment

The lower part of the Tilje Formation is characterised by the overall dominance of tide-generated structures, the scarcity of wave- and storm-generated structures, and a mostly restricted ichnological diversity (Figs 5 to 8). This suggests deposition by a large tide-dominated delta in the semi-enclosed structural embayment that formed within the Early Jurassic Seaway. Paleogeographic reconstructions suggest that deposition of the Tilje Formation occurred within the narrow seaway with

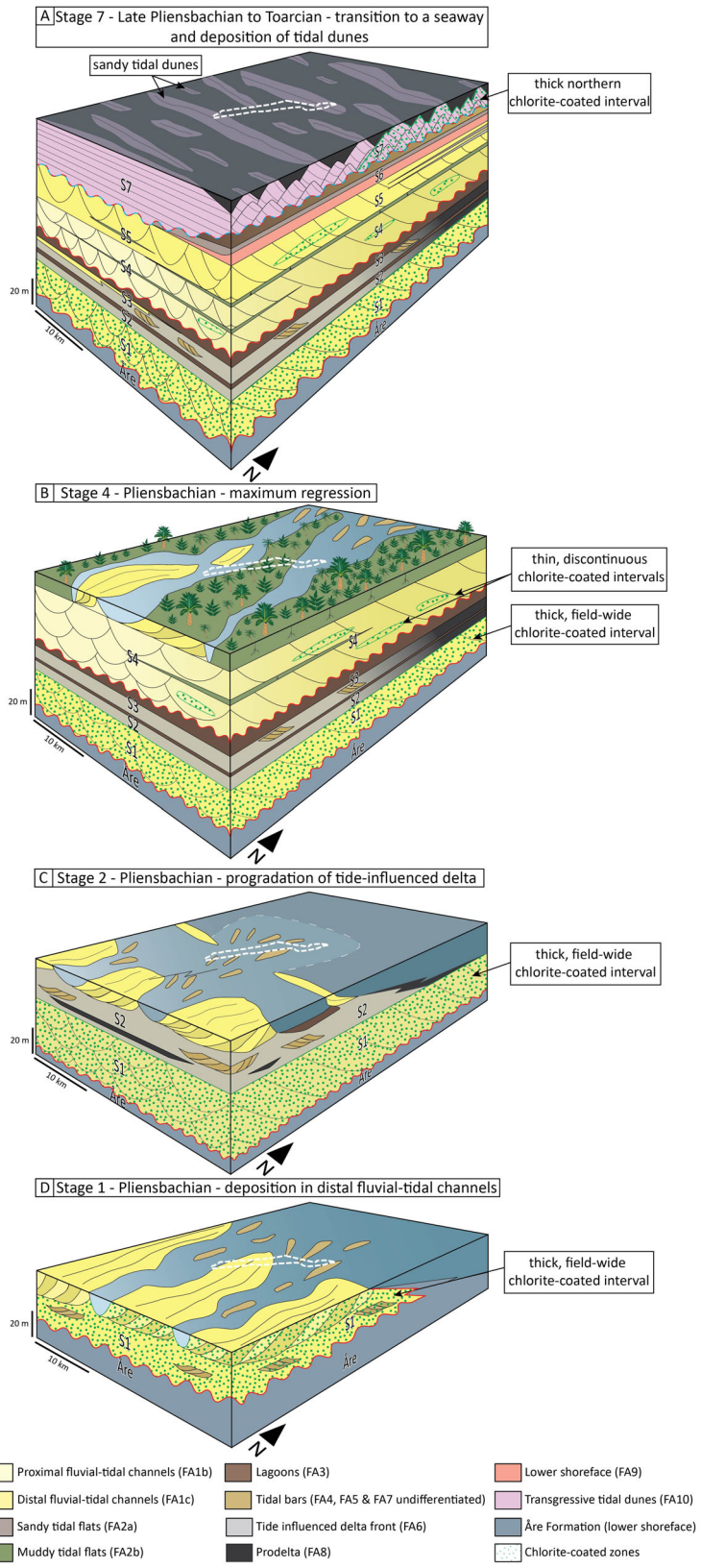

Fig. 9. Model for the deposition of the Tilje system and the distribution of chlorite-coated intervals in (A) Stage 7; (B) Stage 4; (C) Stage 2; (D) Stage 1. The white stippled line shows the approximate location of the Smørbukk Field.

Greenland and the Jan Mayen microcontinent to the west and Mainland Norway to the east (Doré, 1991). Furthermore, seismic sections across the Halten Terrace show that the Tilje Formation forms a generally tabular unit from the Norwegian landmass, onlapping on the Sklinna Ridge to the west (Fig. 3). Therefore, deposition of the Tilje deltaic system occurred in this narrow basin (Fig. 9), contributing to enhancing tidal currents and minimising wave action. Recent studies have shown that tide-dominated deltas in structurally controlled embayments (the Eocene Lower Dir Abu Lifa Member in Egypt; Legler *et al.*, 2013; and the Early Jurassic Gule Horn Formation in eastern Greenland; Eide *et al.*, 2016) display minimal evidence of wave reworking, and these are good analogues for the lower part of the Tilje Formation.

Stages 6 to 7: Deposition of transgressive tidal dunes in a tidal-controlled seaway

A major shift in dominant depositional processes is observed above FS3, where waves and storms become the dominant processes responsible for the deposition of the lower shoreface deposits. These are overlain by erosive-based tidal dune deposits (Stage 7) that record deposition in open-marine settings, as shown by the increase in dinoflagellate cysts and the much more diverse trace fossil assemblage of the *Cruziana* ichnofacies (Figs 5M and 8). Biostratigraphic data place the base of Stage 7 within the very latest Pliensbachian, and the upper part of this unit and the contact to the overlying Ror Formation at or near the Pliensbachian–Toarcian boundary. Field-wide correlation of the erosional contact at the base of Stage 7 highlights significant truncation and removal of underlying units (Fig. 6). Thus, the base of Stage 7 deposits represents a candidate combined sequence boundary and transgressive tidal ravinement surface that records a significant change in the morphology of the basin (Fig. 9) and the abrupt flooding of the Tilje deltaic system. At a North Atlantic rifted seaway scale, regional comparisons indicate this event may be age equivalent to a well-documented phase of intra-latest Pliensbachian relative sea-level fall, tectonics and erosion immediately prior to early Toarcian eustatic sea-level rise, as documented regionally in UK outcrops and on the conjugate margin in East Greenland (Hallam, 1988; Hesselbo & Jenkyns, 1995; Hesselbo *et al.*, 1998: Van Buchem & Knox, 1998; Krencker *et al.*, 2019).

Petrographic analysis

Qualitative analysis of 56 petrographic thin sections has allowed petrographic analysis of several facies associations including distal fluvial-tidal channels (FA1c), sandy and muddy tidal flats (FA2a and FA2b), heterolithic tidal bars (FA4), tide-influenced delta-front (FA6), lower shoreface (FA9) and transgressive tidal dunes (FA10). Grain-coating chlorite occurs mostly in samples of FA1c, facilitating primary porosity preservation (Fig 10A and B). Discontinuous chlorite coats occasionally result in quartz overgrowth, and a few samples show pervasive quartz overgrowth due to the absence of grain-coating chlorite. Feldspar dissolution occasionally leads to secondary porosity (Fig. 10A). Pore-filling kaolinite–chlorite mixed-layer clay precipitation (occurring in less than 8% of the samples) is detrimental to reservoir quality as it blocks pore throats. Samples of FA6 and FA10 occasionally show the occurrence of chlorite coats preserving porosity (Fig 10C to E). However, minor quartz overgrowths or pore-filling kaolinite–chlorite result in reduced porosity (Fig. 10C). Additionally, few samples of FA6 show chlorite coats that are sufficiently thick to occlude pore space (Fig. 10D). Samples of FA2a, FA2b, FA4 and FA9 are characterised by the absence of grain-coating chlorite. This results in extensive quartz cementation and reduced porosity (Fig. 10F).

Permeability analysis

Permeability in the sandstone beds of the Tilje Formation in the Smørbukk Field is typically low (i.e., <1 mD) throughout the studied wells (Fig. 6) because of extensive quartz cementation blocking the pore space (e.g., Fig. 10F). However, up to ca 30 m thick anomalous intervals showing elevated permeability values occur throughout the Smørbukk Field (Fig. 6). These correspond to intervals where permeability is preserved due to the occurrence of chlorite coats around quartz grains, as shown by several thin sections (Figs 10A, B, E and 11D, E, G to I) and highlighted by previous studies (Ehrenberg, 1993; Martinius *et al.*, 2005; Griffiths *et al.*, 2021; Nichols *et al.*, 2025). Critically, as we demonstrate herein, such chlorite-coated intervals showing high permeability can easily be traced in the core because of the colour and friability differences between quartz-cemented intervals (white, hard) and chlorite-coated intervals

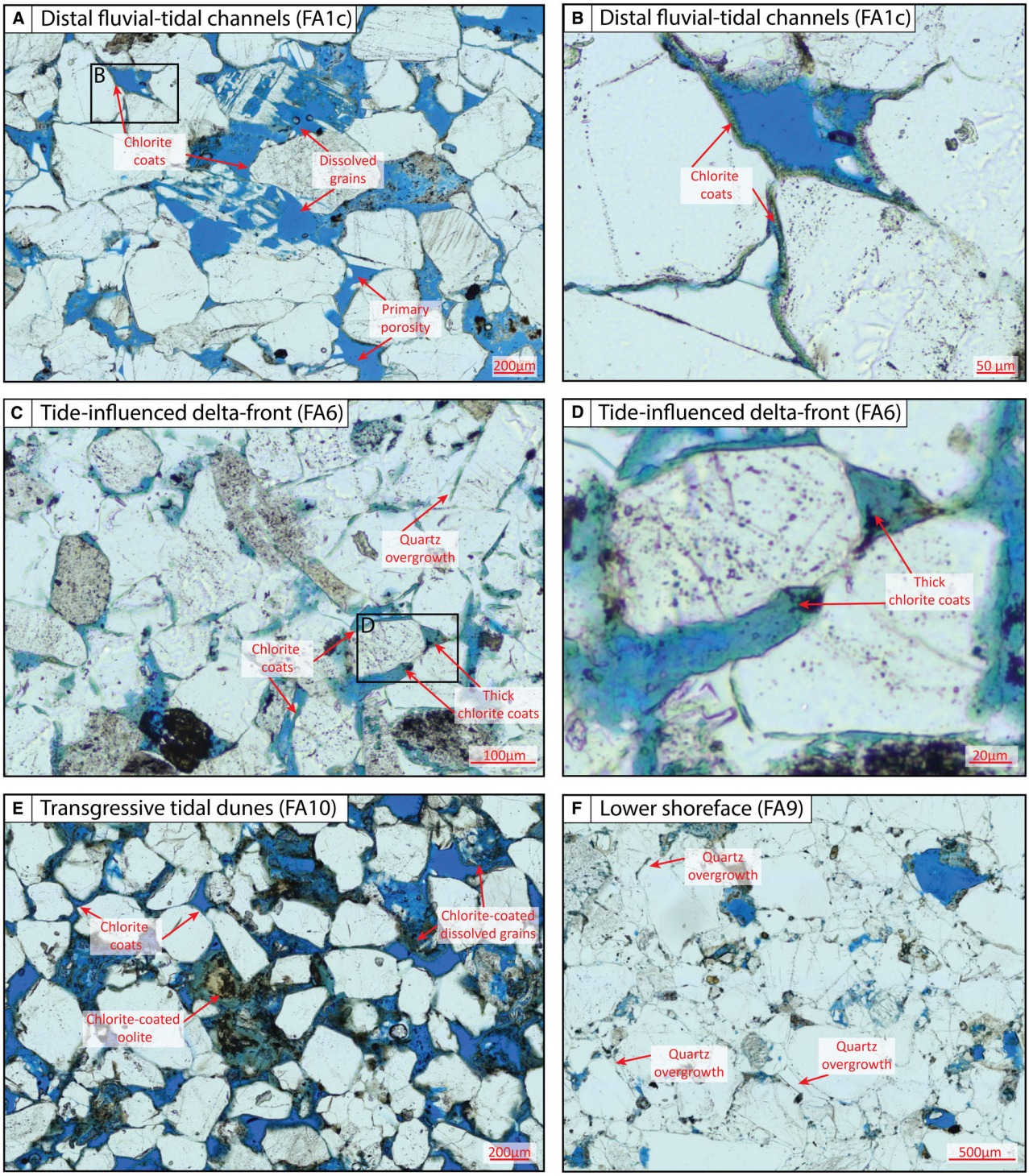

Fig. 10. Petrographic thin sections of samples in (A), (B) distal fluvial-tidal channels (FA1c); (C, D) tide-influenced delta-front (FA6); (E) transgressive tidal dunes (FA10); and (F) lower shoreface (FA9).

(brown, friable; Figs 4 and 11). These distinct intervals occur at different scales (facies association-scale, facies-scale, bed-scale and lamina-scale) and are partly controlled by sedimentological changes (facies, facies association; Fig. 12). In the Tilje Formation, permeability is

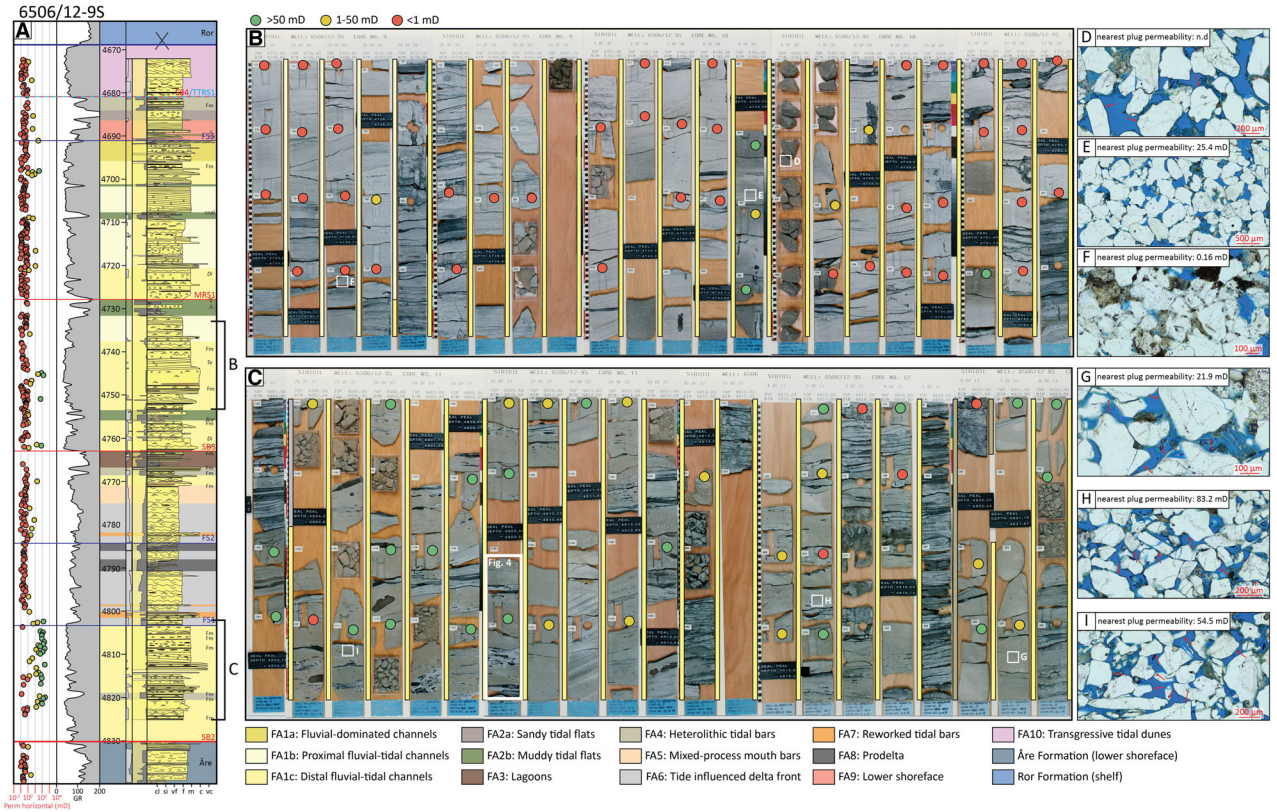

Fig. 11. (A) Sedimentological log of well 6506/12-9S with (from left to right): permeability data (mD; green dots show a permeability higher than 50 mD, yellow dots show a permeability between 1 and 50 mD and red circles show a permeability lower than 1 mD), gamma ray (GAPI), depth (MD), bioturbation index, sandstone/mudstone ratio, sedimentological log with facies associations coloured. Core sections are highlighted in (B) and (C). Permeability data from core plug samples is shown by green, yellow and red circles. Petrographic thin sections are shown in (D to I).

preserved mainly in distal fluvial-tidal channels (FA1c) with strong tidal influence (Fig. 12). Other facies associations such as proximal fluvial-tidal channels (FA1b), sandy tidal flats (FA2a), mixed-process mouth bars (FA5), tide-influenced delta-front (FA6), reworked tidal bars (FA7) and transgressive tidal dunes (FA10) only occasionally show elevated permeability (Fig. 12). Muddy tidal flats (FA2b), lagoons (FA3), heterolithic tidal bars (FA4), prodelta (FA8) and lower shoreface (FA9) show consistent low permeability (Fig. 12), indicating that chlorite coats do not occur in such environments. Furthermore, high permeability is preserved only in a few sedimentary facies: (i) F4.1: coarse- to medium-grained cross-stratified sandstone; (ii) F6.1: coarse- to medium-grained current ripple cross-laminated sandstone; and (iii) F11.3: high-contrast flaser-bedded heterolithic with elongated mudstone clasts (Figs 11 and 12). The other facies show consistent low permeability (<1 mD).

The permeability anomalies can be divided into two categories representing distinct stratigraphic occurrences, mainly based on their thickness and traceability between wells. Thick permeability anomalies show approximately continuously high (>50 mD) permeability for a stratigraphic interval of a few 10's of metres and can be correlated between several wells within the Smørbukk Field (Figs 6, 8, 11 and 12). Thin permeability anomalies show high permeability for a stratigraphic interval of a few metres. These anomalies cannot be traced laterally between several wells (Figs 6 and 8), and are therefore less than a kilometre in lateral length. None of the permeability anomalies described herein can be identified on the 2D seismic presented herein (Fig. 3) as they occur at a scale below seismic resolution.

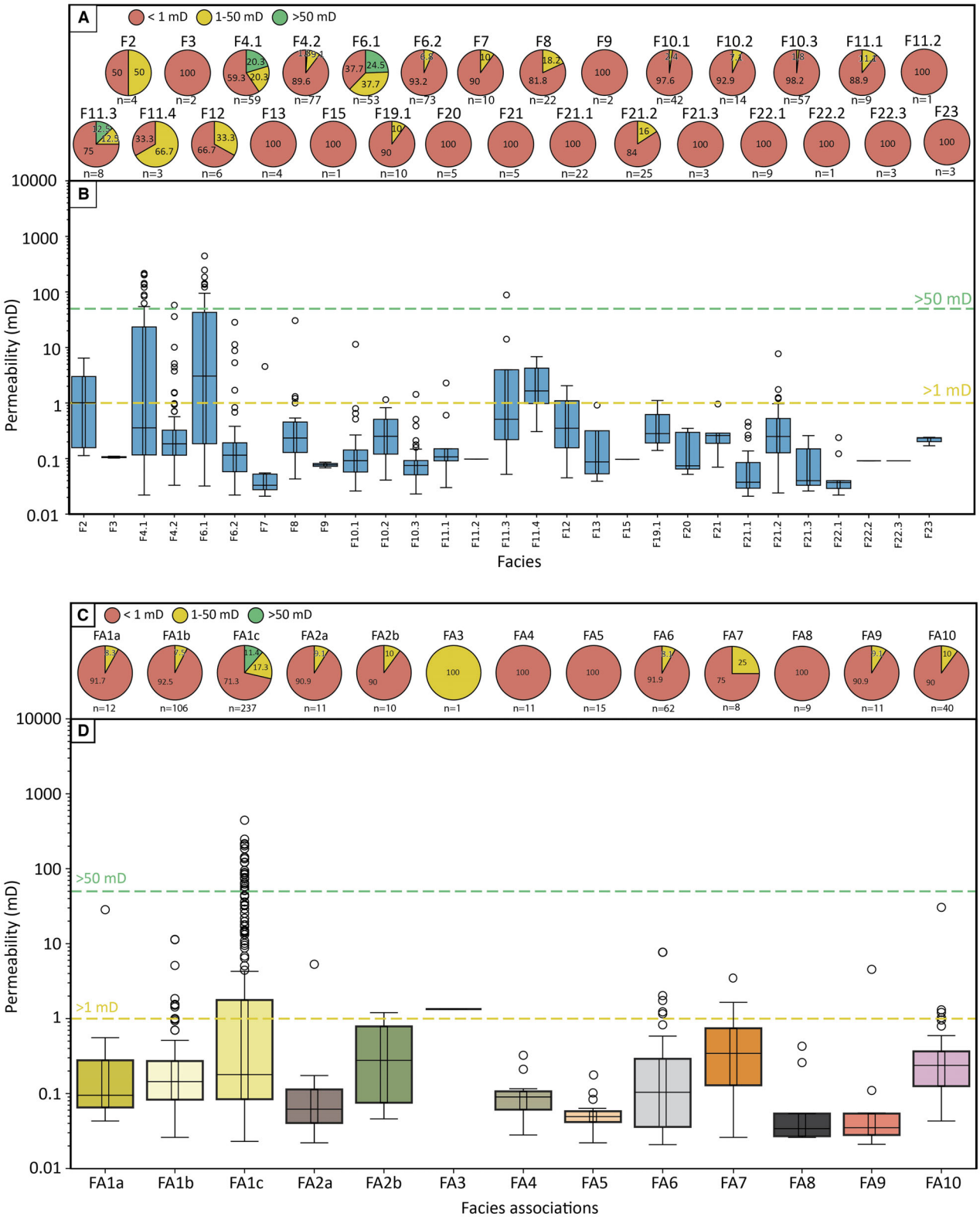

Fig. 12. Percentage of (A) facies and (C) facies associations that show permeability lower than 1 mD (red), between 1 and 50 mD (yellow) and above 50 mD (green); permeability as a function of (B) facies and (D) facies association.

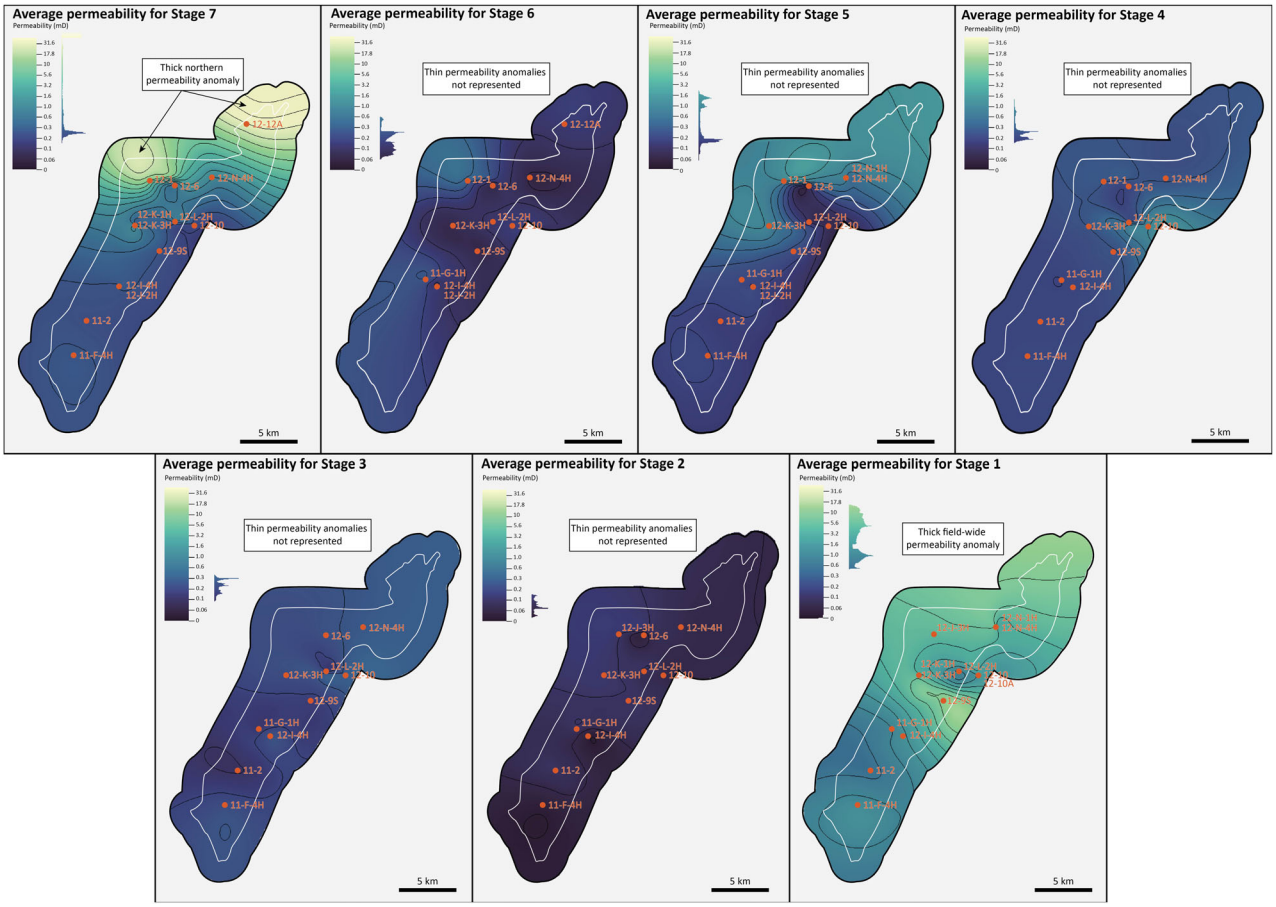

Fig. 13. Average permeability (geometric average) for each stratigraphic Stage. Thin permeability anomalies are not represented because of their thin stratigraphic occurrences. The outline of the Smørbukk Field is shown by a white line.

Thick permeability anomalies

These permeability anomalies are sustained over a significant stratigraphic interval (>10 m) and can be correlated between several wells. This is the case in stratigraphic Stage 1, where an elevated permeability interval of ca. 20 to 30 m thick can be correlated laterally between all investigated wells (ca. 40 km; Figs 6, 8, 9 and 13). This high permeability interval occurs in amalgamated tidal-fluvial channels (FA1c) which make up for most of Stage 1, and it stands out in contrast to the overlying low permeability (<1 mD) bioturbated delta-front heterolithics (FA6) of Stage 2 (Fig. 6). In comparison, the average permeability for Stage 1 is 3.3 mD, with typical high values of 20 to 200 mD. In well 6506/12-9S, there is high permeability for a sustained thickness in the amalgamated tidal-fluvial channels of Stage 1. This interval can be easily identified in the core due to the brown and friable aspect of the cross-bedded and ripple cross-laminated sandstone beds that show high permeability (Fig. 11). These brown friable beds alternate with commonly 5 to 10 cm thick and up to 60 cm thick white, hard intervals that have been extensively quartz-cemented, and show abundant fluid muds and elongated mudstone clasts (F11.1, F11.2 and F11.3; Figs 4 and 11). Critically, this observation indicates that in these intervals, the main property hindering chlorite coating is the proximity to the organic-rich fluid mud layers and organic-rich mudstone clasts. Furthermore, the facies associations which show chlorite coating in Stage 1, occur in other stages where they do not necessarily show elevated permeability and are thus not chlorite-coated. This indicates that facies association is not the only control on chlorite coat presence in

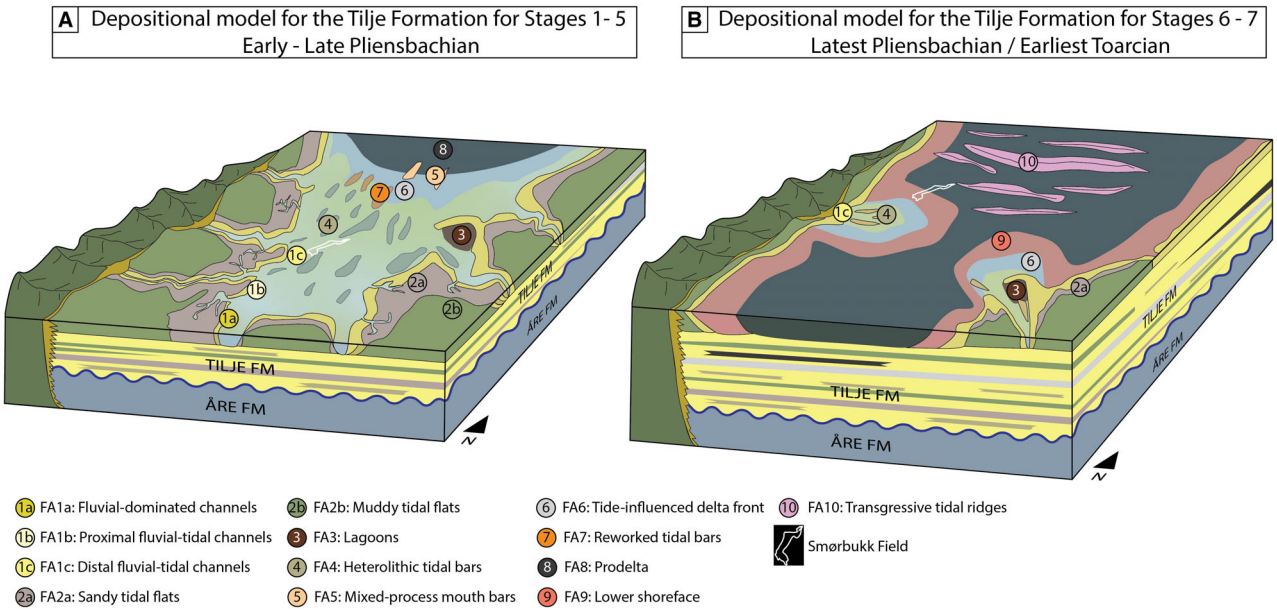

Fig. 14. Paleogeographic reconstruction of the Halten Terrace during the deposition of the Tilje Formation. (A) Early to late Pliensbachian (Stages 1 to 5). (B) Latest Pliensbachian to earliest Toarcian (Stages 6 to 7).

such deeply buried sandstone reservoirs, as the same facies association both show the presence and absence of chlorite-coated intervals.

Additionally, there is a thick high-permeability anomaly in Stage 7 only in the northern part of the Smørbukk Field that can be correlated laterally between 3 wells (ca. 17 km; Figs 8, 9 and 13), in which permeability is preserved for a ca. 10 m thick stratigraphic interval in transgressive tidal dunes (FA10). Permeability is especially high in the northernmost well of the field (6506/12–12A; Fig. 13) with an average of 40 mD for the entire stage, while Stage 7 has an average of 4.3 mD in the entire field, with typical high values of 100 to 1200 mD. This indicates significant regional variations in chlorite coat distribution that occur across the facies association variations, indicating external regional controls such as relative sea-level change, changes in composition of the hinterland, climate, tectonics or geochemical conditions.

Thin permeability anomalies

Thin permeability anomalies also occur in most of the studied wells (Figs 6, 8 and 11), showing high permeability for a thin stratigraphic interval (<3 m). They occur in several stages of the Tilje Formation in fluvial-tidal channels (FA1c), in sandy tidal flats (FA2a), mixed-process mouth bars (FA5), tide-influenced delta-front (FA6) and reworked tidal bars (FA7). They cannot be correlated between several wells and therefore their lateral extent is believed to be less than a kilometre (Fig. 8). Their true lateral dimensions are, however, uncertain due to the lateral limitations of well data. Thin permeability anomalies have an average of 12.6 mD, with typical high values up to ca. 100 mD. These anomalies do not have a noticeable impact when permeability is averaged for an entire stage (Fig. 13) due to their stratigraphically thin occurrence.

DISCUSSION

Comparison with previous studies

Detailed sedimentological investigations of core data from 12 wells have made it possible to refine the understanding of the depositional environments and the stratigraphic architecture of the Tilje Formation in the Smørbukk Field. Previous stratigraphic frameworks (cf.Martinius *et al.*, 2001; Ichaso & Dalrymple, 2014; Ichaso *et al.*, 2016) have divided Tilje Formation into six main reservoir units (T1 to T6; see Fig. 2) and several sub-units (e.g., T1.1.1 and T1.1.2). Several of these units are bounded by sequence boundaries or flooding surfaces and can be correlated for several kilometres.

However, other units merely represent reservoir units (i.e., units with common petrophysical, fluid and/or pressure properties) and do not necessarily have stratigraphic significance. Therefore, this study rather proposes a new division based on stratigraphic units (Stages 1 to 7) bounded by sequence boundaries, major flooding surfaces, maximum regressive surfaces or composite sequence boundary–transgressive tidal ravinement surfaces that can be correlated throughout the Smørbukk Field (Figs 2, 6 and 8). Sequence boundary 2 (SB2) is picked, in accordance with previous studies (Martinius *et al.*, 2001; Ichaso & Dalrymple, 2014; Ichaso *et al.*, 2016), at the abrupt change of facies between fine-grained heterolithic lower shoreface deposits of the Åre Formation and erosive-based fluvial-tidal channels of Stage 1. However, sequence boundary 3 (SB3) is picked at a slightly deeper stratigraphic depth than previous study by Ichaso & Dalrymple (Ichaso & Dalrymple, 2014; Fig. 2). This is supported by the erosional nature of the surface, the sharp grain size change between mudstones below and coarse- to medium-grained sandstones above the surface and an abrupt change of depositional environment between lagoonal deposits below the surface and fluvial-tidal channels above (Figs 2, 6 and 8). Martinius *et al.* (2001) showed that an Nd/Nd isotopic marker below SB3 records a major shift in provenance age between deposits below and above SB3.

The depositional environments of the Tilje Formation defined in this study are in general accordance with previous studies (cf. Martinius *et al.*, 2001; Ichaso & Dalrymple, 2014; Ichaso *et al.*, 2016). However, the uppermost sandstone bodies (Stage 7 in this study, T6 in previous studies) have been previously interpreted as distributary mouth bar deposits (Ichaso & Dalrymple, 2014). Based on evidence described in this study, such as the occurrence of cross-bedded sandstones, the net increase in marine organisms (dinoflagellates) and the more diverse marginal-marine bioturbation, this unit is rather interpreted as having been deposited as compound transgressive tidal dunes away from the fluvial source. The base of this unit is erosive and is likely to represent a composite sequence boundary–transgressive tidal ravinement surface of intra-latest Pliensbachian age (Fig. 8). It is overlain by muddy shelf deposits of the Ror Formation, representing further flooding in the early Toarcian. This has major implications for basin reconstruction and is discussed in the next section.

Paleogeographic implications

Several studies have shown that the Tilje Formation was deposited in an embayment that enhanced tidal processes and minimised wave action (Martinius *et al.*, 2001; Ichaso & Dalrymple, 2014). Seismic sections across the Halten Terrace (see Fig. 3 and Bunkholt *et al.*, 2025) indicate that this embayment was flanked by an emerging provenance area to the west (paleo-Sklinna Ridge) and by the Norwegian landmass to the east (Figs 1, 3 and 14). While a previous study by Ichaso & Dalrymple (2014) in the Smørbukk Field suggests that the most proximal facies occurred in the north of the embayment, a more recent regional study by Bunkholt *et al.* (2025) suggests that the Tilje Formation prograded northwards. The facies trends presented in this study indicate that the most distal facies occur in the north of the Smørbukk Field (Figs 6 to 8), contrasting with the previous interpretation of Ichaso & Dalrymple (2014). This is supported by palynological data that indicated an increase in the abundance of marine organisms in the north of the field, suggesting more frequent marine flooding (Fig. 8). This indicates that the embayment was opened to the north, allowing for occasional reworking by wave and storm processes, especially in the north of the field (Figs 8, 9 and 14). The Smørbukk Field probably lay centrally within the embayment, close to its western margin (Fig. 14), and while the embayment was likely several tens of kilometres wide, the field is ca. 6 km wide. Most of the Tilje Formation (Stage 1 to Stage 6) was likely deposited in this embayment that enhanced tidal currents and favoured the trapping of mud in the basin, resulting in the deposition of highly heterolithic tide-influenced facies. A major shift in basin physiography is here interpreted to have occurred towards the top of the Tilje Formation, with the onset of a late Pliensbachian to early Toarcian regressive-transgressive relative sea-level event causing the basin to evolve from an embayment to a more marine strait setting (Figs 8 and 14). This resulted in an initial incision phase followed by deposition of Stage 7 transgressive tidal dunes and later of heterolithic early Toarcian shelf deposits of the Ror and sandy delta fan deposits of the Tofte Formations (van Cappelle *et al.*, 2017). This event may be age equivalent to the well-documented intra Latest Pliensbachian (*Margaritatus* zone) eustatic sea-level fall, followed by the Early Toarcian eustatic sea-level

rise and warming towards the Toarcian oceanic anoxic event documented elsewhere in the North Atlantic rifted seaway (e.g., Hesselbo & Jenkyns, 1998). Bunkholt *et al.* (2025) however also points to a regional intra-Tilje (latest Pliensbachian) tectonic event during which the North Atlantic rift system propagated northward, resulting in transgression of the Tilje system in the south. Intensified tectonic activity is interpreted to have uplifted local intra basinal highs at this time, while adjacent areas subsided, resulting in a complex depositional pattern across the Halten Terrace (Ichaso *et al.*, 2016; Bunkholt *et al.*, 2025). Regional comparisons to age equivalent outcrop sections in the UK (Hallam, 1988; Hesselbo & Jenkyns, 1995, 1998; Hesselbo *et al.*, 1998; van Buchem & Knox, 1998), East Greenland (Dam & Surlyk, 1998; Ahokas *et al.*, 2014; Eide *et al.*, 2016; Krencker *et al.*, 2019) and subsurface data from the Northern North Sea (Marjanac & Steel, 1997; Charnock *et al.*, 2001) reveal many parallels, with most authors pointing to a combination of eustasy and Atlantic rifted seaway tectonics to drive stratigraphic evolution over the Pliensbachian–Toarcian boundary.

Sedimentological controls on the distribution of chlorite-coated zones

The results of this study suggest that only a few facies and facies associations occasionally preserve relatively high permeabilities due to the occurrence of chlorite coats (Fig. 12). These facies are medium to coarse-grained, cross-bedded or ripple cross-laminated, and mainly 'clean' sandstones (i.e., not heterolithic with a general absence of mudstone drapes, fluid mud layers or mudstone clasts). In some cases, the presence of organic-rich mudstone clasts and fluid mud layers seems to be the main control on the occurrence of chlorite coating (Figs 4 and 11). These facies were deposited by medium- to high-energy uni- or bidirectional flows due to ripple or dune migration, suggesting that these depositional processes might be favourable to the formation of chlorite coats. However, these coarse-grained and clean sandstone facies are likely to be the facies that would have preserved high porosity and permeability in the primary depositional environment. Therefore, as discussed by Gould *et al.* (2010), the present high permeability of these facies cannot be used as a guide to early diagenetic conditions. Additionally, the preservation of high permeability in these facies only occurs occasionally and not systemically, suggesting that facies is not the only control on the preservation of high permeability due to the occurrence of chlorite coats.

Recent studies on the occurrence of chlorite coats in the subsurface have shown that the optimum conditions for developing chlorite coating occur in tidal-fluvial bars (Virolle *et al.*, 2019b; Griffiths *et al.*, 2021). The results of this study show that chlorite-coated zones mainly occur in distal fluvial-tidal channels (FA1c; Figs 8, 9 and 12). However, chlorite-coated zones also occur in other depositional environments, like transgressive tidal dunes (FA10) in the north of the Smørbukk Field (Figs 8, 9, 12 and 13). These depositional environments represent high-energy settings where tidal processes are dominant. Conversely, intervals where wave and storm actions are the dominant depositional processes do not show high permeability (Figs 6, 8 and 13). This indicates that tidal processes are favourable to the development of chlorite-coated intervals, likely because tidal processes are efficient at reworking sediments and serve as an effective mechanism for the distribution and development of precursor clay coats. The heterogeneous distribution of chlorite coats in distal fluvial-tidal channels, especially in Stages 4 and 5, could reflect differential reworking and/or precursor clay material availability.

Although chlorite-coated zones often occur within distal fluvial-tidal channels, the geometry of these zones varies greatly throughout the Tilje Formation (Figs 8 and 9), and this greatly impacts reservoir connectivity. Thick (ca. 20 m), stratigraphically bounded chlorite-coated zones occur within Stage 1 and Stage 7 in the north of the field, while thin (ca. 2 m), discontinuous zones occur within Stages 2 to 5. These anomalies occur within similar facies and facies associations, and it is therefore difficult to recognise subtle differences in depositional processes. However, Stages 4 and 5 represent the most proximal stages of the system and show overall a greater influence of fluvial processes. This might have been detrimental to the development of chlorite coats either because tidal processes were too weak to efficiently bring precursor clay minerals or because the fluvial energy was too high to deposit the finer grain size fractions. The thick chlorite-coated intervals of Stages 1 and 7 occur within transgressive cycles and above regressive cycles and sequence boundaries (Fig. 8). Therefore, fluctuations in relative sea-level could explain

differences in the distribution of chlorite-coated intervals, where transgressive cycles favour the reworking of precursor clay coats and thus the development of chlorite-coated intervals, as previously suggested by Morad *et al.* (2010).

Other controls on the distribution of chlorite-coated zones

Although this study shows that depositional processes and depositional environments are key factors partially controlling the distribution of chlorite-coated zones in the subsurface, they do not fully explain the distribution of chlorite in the Tilje Formation. Therefore, other controlling factors must be considered. Assuming that chlorite coats are formed by the recrystallisation of precursor clay minerals (Ehrenberg, 1993; Aagaard *et al.*, 2000; Ajdukiewicz *et al.*, 2010), the distribution of chlorite coats in the subsurface is controlled by the distribution of these clay minerals or their precursors in the primary depositional environment and the capacity to remobilise and attach these clay minerals to sand grains (Wooldridge *et al.*, 2017; Worden *et al.*, 2020; Haile *et al.*, 2022). Ehrenberg (1993) proposed two mechanisms for forming precursor clay minerals in high-energy sandstones: (i) these formed in a favourable environment elsewhere and were introduced in the sand by reworking; and (ii) they mineralised within the sand due to local favourable geochemical conditions. If these two mechanisms for forming precursor clay minerals co-occurred within the Tilje Formation, they could have resulted in differences in the distribution of chlorite coats and therefore in the two types of chlorite-coated zones observed throughout the Formation (Figs 8 and 9).

Studies have shown that precursor clay minerals such as odinite form in shallow prodelta and shelf settings (Odin & Fullagar, 1988), and Griffiths *et al.* (2021) postulated that chlorite precursors could form in lagoonal settings. A recent study by Jahren *et al.* (2025) suggests that the formation of iron-rich precursor clay minerals can occur in shelf- to lower shoreface settings, in the 'chlorite kitchen facies'. These precursor clay minerals might be later reworked by storm processes, incorporated within more proximal sandy environments, and eventually be attached to sand grains and recrystallise to form precursor clay coats. Lower shoreface deposits of the Åre Formation, below Stage 1, and lower shoreface deposits of Stage 6, below Stage 7, might thus be favourable environments for the formation of precursor clay minerals. It is therefore possible that tidal currents that were dominant in Stage 1 and Stage 7 reworked these lower shoreface deposits, incorporating large amounts of precursor clay minerals within the fluvial-tidal channels of Stage 1, eventually leading to the development of thick chlorite-coated zones (Fig. 8). Conversely, Stage 4 and Stage 5 were not deposited in proximity to lower shoreface deposits favourable for the formation of precursor clay minerals, and therefore rather depended on local favourable geochemical conditions within the sands for forming precursors clay minerals (mechanism two; Ehrenberg, 1993). This could have resulted in the patchy distribution of chlorite-coated zones observed in Stage 4 and Stage 5 (Figs 8 and 9). In this case, the occurrence and distribution of chlorite coats might be controlled by the proximity to the favourable environment for forming precursor clay minerals (i.e., lower shoreface or shelf) and by the ability to rework and incorporate these precursor clay minerals. This might also depend on changes in relative sea-level, as transgressive cycles are more efficient in reworking and mixing fine-grained material (Saïag *et al.*, 2016). Therefore, the development of thick chlorite-coated zones in the Smørbukk Field likely depends on a combination of factors, including depositional processes (facies, facies association) dominant at the time of deposition, as well as depositional processes in adjacent environments and the ability to rework previously deposited material during, for example, relative sea-level rise.

Several Lower to Middle Jurassic formations of the NCS show chlorite-rich intervals (e.g., the Tilje and Tofte formations; Ehrenberg, 1990, 1993; the Cook Formation; Marjanac & Steel, 1997; Aagaard *et al.*, 2000; Charnock *et al.*, 2001; Folkestad & Steel, 2023). This suggests that conditions favourable to the development of chlorite coats occurred regionally in this period. Therefore, regionally controlled factors such as the composition of provenance material might be key to developing chlorite-coated zones. Several sediment sources might have been active at different times throughout the deposition of the Tilje Formation (Morton *et al.*, 2009; Bunkholt *et al.*, 2025). Differences in the composition of the sediment source control the supply of iron into the sedimentary system and therefore influence the availability of precursor clay minerals in the system (Worden *et al.*, 2020). This might

result in differences in the distribution of chlorite-coated zones in the Tilje Formation. This possibility needs to be investigated by a high-resolution provenance study to understand possible variations in sand provenances throughout the Formation and the basin.

The exact mechanism for forming chlorite coats in the Jurassic Formations of the NCS remains uncertain (Ehrenberg, 1993), but it is known that favourable geochemical conditions are necessary for forming precursor clay minerals that will recrystallise to chlorite (Jahren *et al.*, 2025). The cool temperatures in the early to middle Pliensbachian were followed by a major warming interval during the early Toarcian oceanic anoxic event (Scotese *et al.*, 2021). Such oceanic anoxic events affect the global carbon cycle, causing major changes in ocean chemistry (Jenkyns, 2010). However, the effects of such regional geochemical and climatic events on chlorite formation, when coupled to the well-documented high-frequency eustatic cycles in the Pliensbachian to Toarcian time intervals (Hallam, 1988, 1997; Hesselbo & Jenkyns, 1995, 1998; Hesselbo *et al.*, 1998; Van Buchem & Knox, 1998), have yet to be investigated. Furthermore, chlorite-rich ooids and ironstones are commonly described across several Lower to Middle Jurassic sedimentary successions of the North Atlantic rifted seaway (e.g., in the Cleveland Basin, England; Hesselbo & Jenkyns, 1995, 1998; van Buchem & Knox, 1998; Powell, 2010; the Hebrides of Skye and Raasay, Scotland; Morton, 1965; Hesselbo *et al.*, 1998; in Liverpool Land, East Greenland; Surlyk *et al.*, 2021). This suggests that a favourable Early- to Middle Jurassic climate is likely to have contributed to the distribution of iron-rich chlorite precursors on a regional scale across sub-basins of the North Atlantic Seaway. Data from the Cleveland Basin and adjacent areas may be particularly informative as they document examples of both *in situ* chlorite formation developed on intrabasinal highs (chamositic/limonitic oolite successions), and reworking of material from these highs into adjacent basins and incorporation with shelfal clastics (van Buchem & Knox, 1998; Powell, 2010). These studies suggest that Jurassic oolitic ironstones in Europe preferentially accumulated during periods of condensation in shallow water on, or adjacent to, densely vegetated landmasses that underwent lateritic weathering during periods of reduced sediment influx.

CONCLUSION

Ten facies associations (FA1 to FA10) have been defined in the Tilje Formation in the Smørbukk Field, on the basis of sedimentological, ichnological and palynological data. Most of the investigated deposits are highly heterolithic, showing abundant mudstone drapes and fluid muds and a restricted trace fossil assemblage, recording the evidence of tide action. The lower part of the Tilje Formation (Stages 1 to 5) is interpreted as being deposited in a large aggrading and later prograding tide-influenced delta, showing river influence and weak wave influence. The upper part of the Tilje Formation (Stages 6 and 7) is interpreted as the deposits of transgressive shorefaces and tidal dunes.

The highly heterolithic nature of the Tilje Formation, and the general scarcity of wave- and storm-generated structures indicate that sedimentation occurred in a large structural embayment, resulting in a high amount of mud available for deposition and enhanced tidal currents. The most distal facies occur in the north of the Smørbukk Field, suggesting that the embayment was opened to the north, and this allowed occasional reworking by wave and storm processes. This large deltaic system was progressively transgressed, resulting in the deposition of wave- and storm-influenced deposits and transgressive tidal dunes. This shift to more marginal-marine conditions towards the top of the Tilje Formation reflects the progressive opening of the embayment to the south and further deposition in a tidal-dominated strait. Biostratigraphic data indicate this event is of intra-latest Pliensbachian to early Toarcian age, and likely correlates to a pronounced phase of tectonism and high-frequency eustatic change within the North Atlantic rifted seaway.

The Tilje Formation is buried to ca. 5 km in the Smørbukk Field, resulting in extensive quartz cementation and therefore very low permeability, except in zones that show chlorite coats preserving high permeability down to ca. 5 km. Chlorite coats mainly occur in coarse-grained sandstone facies, suggesting that they develop in high-energy settings. Additionally, chlorite coats occur preferentially in transgressive cycles in distal tidal-fluvial channels and tidal dunes, suggesting that tidal currents and rises in relative sea-level play an important role in reworking and mixing chlorite precursor minerals with coarse-grained sands. Wave-dominated environments and proximal fluvial-tidal channels do not develop chlorite coats.

For the first time, this study highlights the lateral and vertical distribution of chlorite-coated zones in the subsurface and shows that the geometry of such zones varies greatly within the Tilje Formation between thick stratigraphically bounded zones and thin laterally discontinuous zones. Such chlorite-coated zones occur within the same facies and facies associations, indicating that sedimentological controls do not fully explain the distribution of chlorite in the subsurface, and that other regional controls such as provenance, climate, tectonics, eustasy and geochemical conditions in the primary depositional environments have to be considered. Hence, the results presented in this study are a valuable first step for understanding the distribution and geometry of chlorite-coated zones in the subsurface.

ACKNOWLEDGEMENTS

This work was conducted as part of the Deep Reservoir project, funded by the Norwegian Research Council (grant 336440), and supported financially by Aker BP ASA, DNO ASA and Equinor ASA. We thank Joshua Griffiths and Frans van Buchem for their constructive reviews that improved the quality of this manuscript, and Marcos Aurell for editorial comments. We also thank Albina Gilmullina and William Helland-Hansen for constructive discussions and feedback on parts of this manuscript. The Norwegian Offshore Directorate is acknowledged for allowing access to core material. Equinor ASA is thanked for giving permission to utilise biostratigraphic and biofacies data. TGS is acknowledged for access to the Facies Map Browser (FMB) database and to 2D seismic data through the DISKOS database. We also thank Leo Zijerveld for facilitating access to DISKOS data.

CONFLICT OF INTEREST

The authors declare no conflict of interest.

DATA AVAILABILITY STATEMENT

The data that supports the findings of this study are available from the Norwegian National Data Repository for petroleum data from DISKOS (https://www.sodir.no/en/diskos). Restrictions apply to the availability of biostratigraphic and biofacies data, which were used under a licence for the current study and are not publicly available.

REFERENCES

Aagaard, P., **Jahren, J.S.**, **Harstad, A.O.**, **Nilsen, O.** and **Ramm, M.** (2000) Formation of grain-coating chlorite in sandstones. Laboratory synthesized vs. natural occurrences. *Clay Mineral.*, **35**, 261–269.

Ahokas, J.M., **Nystuen, J.P.** and **Martinius, A.W.** (2014) Stratigraphic signatures of punctuated rise in relative sea-level in an estuary-dominated heterolithic succession: Incised valley fills of the Toarcian Ostreaelv Formation, Neill Klinter Group (Jameson Land, East Greenland). *Mar. Petrol. Geol.*, **50**, 103–129.

Ajdukiewicz, J.M., **Nicholson, P.H.** and **Esch, W.L.** (2010) Prediction of deep reservoir quality using early diagenetic process models in the Jurassic Norphlet Formation, Gulf of Mexico. *AAPG Bull.*, **94**, 1189–1227.

Arnott, R.W. and **Southard, J.B.** (1990) Exploratory flow-duct experiments on combined-flow bed configurations, and some implications for interpreting storm-event stratification. *J. Sed. Res.*, **60**, 211–219.

van den Berg, J.H., **Boersma, J.R.** and **van Gelder, A.** (2007) Diagnostic sedimentary structures of the fluvial-tidal transition zone – Evidence from deposits of the Rhine and Meuse. *Neth. J. Geosci. Geol. Mijnbouw*, **86**, 287–306.

Billault, V., **Beaufort, D.**, **Baronnet, A.** and **Lacharpagne, J.-C.** (2003) A nanopetrographic and textural study of grain-coating chlorites in sandstone reservoirs. *Clay Mineral.*, **38**, 315–328.

Blakey, R. (2021) Paleotectonic and paleogeographic history of the Arctic region. *Atlantic Geosci.*, **57**, 7–39.

Bloch, S., **Lander, R.H.** and **Bonnell, L.** (2002) Anomalously high porosity and Permeability in deeply buried sandstone reservoirs: Origin and predictability. *AAPG Bull.*, **86**, 301–328.

Blystad, P., **Brekke, H.**, **Færseth, R.B.**, **Larsen, B.T.**, **Skogseid, J.** and **Tørudbakken, B.** (1995) Structural elements of the Norwegian continental shelf. Part II: The Norwegian Sea Region. *Norw. Petrol. Direct. Bull.*, **8**, 45.

Boersma, J.R. (1969) Internal structures of some tidal megaripples on a shoal in the Westerschelde estuary, The Netherlands. *Geol. Mijnbouw*, **48**, 409–414.

van Buchem, F.S.P. and **Knox, R.** (1998) Lower and Middle Liassic depositional sequences of Yorkshire (U.K.). In: *Mesozoic and Cenozoic Sequence Stratigraphy of European Basins* (Eds de Graciansky, P.-C., Hardenbol, J., Jacquin, T. and Vail, P.R.), Vol. **60**, pp. 545–559. *SEPM Special Publication*.

Bunkholt, H.S.S., **Oftedal, B.T.**, **Hansen, J.A.**, **Løseth, H.** and **Kløvjan, O.S.** (2025) Trøndelag platform and Halten–Dønna terraces composite tectono-sedimentary element, Norwegian rifted margin, Norwegian sea. *Geol. Soc. London Mem.*, **57**, M57-2017-2013.

van Cappelle, M., **Stukins, S.**, **Hampson, G.J.** and **Johnson, H.D.** (2016) Fluvial to tidal transition in proximal, mixed tide-influenced and wave-influenced deltaic deposits: Cretaceous lower Sego Sandstone, Utah, USA. *Sedimentology*, **63**, 1333–1361.

van Cappelle, M., **Ravnås, R.**, **Hampson, G.J.** and **Johnson, H.D.** (2017) Depositional evolution of a progradational to

aggradational, mixed-influenced deltaic succession: Jurassic Tofte and Ile formations, southern Halten Terrace, offshore Norway. *Mar. Petrol. Geol.*, **80**, 1–22.

Charnock, M.A., **Kristiansen, I.L.**, **Ryseth, A.** and **Fenton, J.P.G.** (2001) Sequence stratigraphy of the Lower Jurassic Dunlin Group, northern North Sea. *Norw. Petrol. Soc. Spec. Publ.*, **10**, 145–174.

Cheng, J., **Yu, H.**, **Liu, N.**, **Yu, Y.**, **Ahmat, K.** and **Zhao, R.** (2022) Experimental investigation for the impact of chlorite dissolution on CO_2 mineral trapping in a sandstone-brine-CO_2 system. *Greenhous. Gas. Sci. Technol.*, **12**, 470–485.

Dalland, A., **Worsley, D.** and **Ofstad, K.** (1988) A lithostratigraphic scheme for the Mesozoic and Cenozoic succession offshore mid and northern Norway. *Norw. Petrol. Direct. Bull.*, **4**, 65.

Dalrymple, R.W. and **Rhodes, R.N.** (1995) Chapter 13 Estuarine dunes and bars. In: *Developments in Sedimentology* (Ed Perillo, G.M.E.), Vol. **53**, pp. 359–422. Elsevier, London.

Dalrymple, R.W., **Kurcinka, C.E.**, **Jablonski, B.V.J.**, **Ichaso, A.A.** and **Mackay, D.A.** (2015) Chapter 1 – Deciphering the relative importance of fluvial and tidal processes in the fluvial–marine transition. In: *Developments in Sedimentology* (Eds Ashworth, P.J., Best, J.L. and Parsons, D.R.), Vol. **68**, pp. 3–45. Elsevier, London.

Dam, G. and **Surlyk, F.** (1998) Stratigraphy of the Neill Klinter Group; a Lower – lower Middle Jurassic tidal embayment succession, Jameson Land, East Greenland. *Geol. Greenl. Surv. Bull.*, **175**, 5026.

Doré, A.G. (1991) The structural foundation and evolution of Mesozoic seaways between Europe and the Arctic. *Palaeogeogr. Palaeoclimatol. Palaeoecol.*, **87**, 441–492.

Doré, A.G., **Lundin, E.R.**, **Jensen, L.N.**, **Birkeland, Ø.**, **Eliassen, P.E.** and **Fichler, C.** (1999) Principal tectonic events in the evolution of the northwest European Atlantic margin. *Geol. Soc. London Petrol. Geol. Conf. Ser.*, **5**, 41–61.

Dumas, S. and **Arnott, R.W.C.** (2006) Origin of hummocky and swaley cross-stratification – The controlling influence of unidirectional current strength and aggradation rate. *Geology*, **34**, 1073–1076.

Ehrenberg, S. (1990) Relationship between diagenesis and reservoir quality in sandstones of the Garn Formation, Haltenbanken, mid-Norwegian continental shelf. *AAPG Bull.*, **74**, 1538–1558.

Ehrenberg, S.N. (1993) Preservation of anomalously high porosity in deeply buried sandstones by grain-coating chlorite: Examples from the Norwegian Continental Shelf1. *AAPG Bull.*, **77**, 1260–1286.

Ehrenberg, S.N., **Dalland, A.**, **Nadeau, P.H.**, **Mearns, E.W.** and **Amundsen, E.F.** (1998) Origin of chlorite enrichment and neodymium isotopic anomalies in Haltenbanken sandstones. *Mar. Petrol. Geol.*, **15**, 403–425.

Eide, C.H., **Howell, J.A.**, **Buckley, S.J.**, **Martinius, A.W.**, **Oftedal, B.T.** and **Henstra, G.A.** (2016) Facies model for a coarse-grained, tide-influenced delta: Gule Horn Formation (early Jurassic), Jameson Land, Greenland. *Sedimentology*, **63**, 1474–1506.

Faleide, J.I., **Tsikalas, F.**, **Breivik, A.J.**, **Mjelde, R.**, **Ritzmann, O.**, **Engen, Ø.**, **Wilson, J.** and **Eldholm, O.** (2008) Structure and evolution of the continental margin off Norway and the Barents Sea. *Episodes*, **31**, 82–91.

Folkestad, A. and **Steel, R.J.** (2023) A new interpretation for the Pliensbachian Cook Formation (northern North Sea) as north–south-prograding tidal deltas and shelf ridges in the Early Jurassic Seaway: New model of linkage to the Norwegian Sea. *Geol. Soc. London Spec. Publ.*, **523**, 329–367.

General Bathymetric Chart of the Oceans. (2024) GEBCO_2024 Grid. https://www.gebco.net/data-products-gridded-bathymetry-data/gebco2024-grid.

Gingras, M.K. and **MacEachern, J.A.** (2012) Tidal ichnology of shallow-water clastic settings. In: *Principles of Tidal Sedimentology* (Eds Davis, R.A. and Dalrymple, R.W.), pp. 57–77. Springer Netherlands, Dordrecht.

Gingras, M.K., **MacEachern, J.A.**, **Dashtgard, S.E.** and **Bann, K.L.** (2025) The *Teichichnus* Ichnofacies: Its neoichnological basis and identification in the rock record. *Sedimentology*, **72**, 408–441.

Gould, K., **Pe-Piper, G.** and **Piper, D.J.W.** (2010) Relationship of diagenetic chlorite rims to depositional facies in Lower Cretaceous reservoir sandstones of the Scotian Basin. *Sedimentology*, **57**, 587–610.

Griffiths, J., **Worden, R.H.**, **Wooldridge, L.J.**, **Utley, J.E.P.**, **Duller, R.A.** and **Edge, R.L.** (2019) Estuarine clay mineral distribution: Modern analogue for ancient sandstone reservoir quality prediction. *Sedimentology*, **66**, 2011–2047.

Griffiths, J., **Worden, R.H.**, **Utley, J.E.P.**, **Brostrøm, C.**, **Martinius, A.W.**, **Lawan, A.Y.** and **Al-Hajri, A.I.** (2021) Origin and distribution of grain-coating and pore-filling chlorite in deltaic sandstones for reservoir quality assessment. *Mar. Petrol. Geol.*, **134**, 105326.

Gugliotta, M., **Kurcinka, C.E.**, **Dalrymple, R.W.**, **Flint, S.S.** and **Hodgson, D.M.** (2016) Decoupling seasonal fluctuations in fluvial discharge from the tidal signature in ancient deltaic deposits: An example from the Neuquén Basin, Argentina. *J. Geol. Soc. London*, **173**, 94–107.

Gugliotta, M., **Saito, Y.**, **Nguyen, V.L.**, **Ta, T.K.O.**, **Nakashima, R.**, **Tamura, T.**, **Uehara, K.**, **Katsuki, K.** and **Yamamoto, S.** (2017) Process regime, salinity, morphological, and sedimentary trends along the fluvial to marine transition zone of the mixed-energy Mekong River delta, Vietnam. *Cont. Shelf Res.*, **147**, 7–26.

Guy-Ohlson, D. (1992) Botryococcus as an aid in the interpretation of palaeoenvironment and depositional processes. *Rev. Palaeobot. Palynol.*, **71**, 1–15.

Haile, B.G., **Hansen, H.N.**, **Aagaard, P.** and **Jahren, J.** (2022) How do chlorite coatings form on quartz surface? *J. Petrol. Sci. Eng.*, **215**, 110682.

Hallam, A. (1988) A reevaluation of Jurassic eustasy in the light of new data and the revised Exxon curve. In: *Sea-Level Changes: An Integrated Approach* (Eds Wilgus, C.K., Hastings, B.S., Posamentier, H., Van Wagoner, J., Ross, C.A. and Kendall, C.G.S.C.), Vol. **42**, *SEPM Special Publication*.

Hallam, A. (1997) Estimates of the amount and rate of sea-level change across the Rhaetian–Hettangian and Pliensbachian–Toarcian boundaries (latest Triassic to early Jurassic). *J. Geol. Soc. London*, **154**, 773–779.

Heald, M.T. and **Larese, R.E.** (1974) Influence of coatings on quartz cementation. *J. Sed. Res.*, **44**, 1269–1274.

Hesselbo, P. and **Jenkyns, H.C.** (1995) A comparison of the Hettangian to Bajocian successions of Dorset and Yorkshire. In: *Field Geology of the British Jurassic* (Ed Taylor, P.D.), pp. 105–150. Geological Society of London, London.

Hesselbo, P. and **Jenkyns, H.C.** (1998) British Lower Jurassic sequence stratigraphy. In: *Mesozoic and Cenozoic*

Sequence Stratigraphy of European Basins (Eds de Graciansky, P.-C., Hardenbol, J., Jacquin, T. and Vail, P.R.), Vol. **60**, pp. 561–581. *SEPM Special Publication*.

Hesselbo, P., **Oates, M.J.** and **Jenkyns, H.C.** (1998) The lower Lias Group of the Hebrides Basin. *Scott. J. Geol.*, **34**, 23–60.

Ichaso, A.A. and **Dalrymple, R.W.** (2009) Tide- and wave-generated fluid mud deposits in the Tilje Formation (Jurassic), offshore Norway. *Geology*, **37**, 539–542.

Ichaso, A.A. and **Dalrymple, R.W.** (2014) Eustatic, tectonic and climatic controls on an early syn-rift mixed-energy delta, Tilje Formation (Early Jurassic, Smørbukk field, offshore mid-Norway). In: *From Depositional Systems to Sedimentary Successions on the Norwegian Continental Margin* (Eds Martinius, A.W., Ravnås, R., Howell, J.A., Steel, R.J. and Wonham, J.P.), pp. 339–388. John Wiley & Sons, Hoboken.

Ichaso, A.A., **Dalrymple, R.W.** and **Martinius, A.W.** (2016) Basin analysis and sequence stratigraphy of the synrift Tilje Formation (Lower Jurassic), Halten terrace giant oil and gas fields, offshore mid-Norway. *AAPG Bull.*, **100**, 1329–1375.

Jahren, J., **Haile, B.G.**, **Hansen, H.N.** and **Aagaard, P.** (2025) The Chlorite-Coat Facies-Chemical and Physical Considerations. Available at SSRN 5386695.

Jenkyns, H.C. (2010) Geochemistry of oceanic anoxic events. *Geochem. Geophys. Geosyst.*, **11**, 2788.

Krencker, F.-N., **Lindström, S.** and **Bodin, S.** (2019) A major sea-level drop briefly precedes the Toarcian oceanic anoxic event: Implication for Early Jurassic climate and carbon cycle. *Sci. Rep.*, **9**, 12518.

Legler, B., **Johnson, H.D.**, **Hampson, G.J.**, **Massart, B.Y.**, **Jackson, C.A.L.**, **Jackson, M.D.**, **El-Barkooky, A.** and **Ravnas, R.** (2013) Facies model of a fine-grained, tide-dominated delta: lower Dir Abu Lifa Member (Eocene), Western Desert, Egypt. *Sedimentology*, **60**, 1313–1356.

MacEachern, J.A. and **Bann, K.L.** (2020) The *Phycosiphon* Ichnofacies and the *Rosselia* Ichnofacies: Two new ichnofacies for marine deltaic environments. *J. Sed. Res.*, **90**, 855–886.

MacEachern, J.A. and **Bann, K.L.** (2023) Departures from the archetypal deltaic ichnofacies. In: *Ichnology in Shallow-Marine and Transitional Environments*. (Eds Cónsole-Gonella, C., de Valais, S., Díaz-Martínez, I., Citton, P., Verde, M. and Mcllroy, D.), Vol. **522**, pp. 175–213. *Geological Society, London, Special Publications*.

MacEachern, J.A., **Bann, K.L.**, **Pemberton, S.G.** and **Gingras, M.K.** (2007) The ichnofacies paradigm: High-resolution paleoenvironmental interpretation of the rock record. In: *Applied Ichnology* (Eds MacEachern, J.A., Bann, K.L., Gingras, M.K. and Pemberton, S.G.), Vol. **52**, *SEPM Society for Sedimentary Geology*.

MacEachern, J.A., **Pemberton, S.**, **Gingras, M.**, **Bann, K.**, **James, N.** and **Dalrymple, R.** (2010) Ichnology and facies models. In: *Facies Models: 4* (Eds James, N.P. and Dalrymple, R.W.). Geological Association of Canada, St. John's, NL.

MacKay, D.A. and **Dalrymple, R.W.** (2011) Dynamic mud deposition in a tidal environment: The record of fluid-mud deposition in the Cretaceous Bluesky Formation, Alberta, Canada. *J. Sed. Res.*, **81**, 901–920.

Marjanac, T. and **Steel, J.R.** (1997) Dunlin Group sequence stratigraphy in the northern North Sea: A model for cook sandstone deposition. *AAPG Bull.*, **81**, 276–292.

Marsh, N., **Imber, J.**, **Holdsworth, R.E.**, **Brockbank, P.** and **Ringrose, P.** (2010) The structural evolution of the Halten Terrace, offshore Mid-Norway: extensional fault growth and strain localisation in a multi-layer brittle–ductile system. *Basin Res.*, **22**, 195–214.

Martinius, A.W., **Kaas, I.**, **Næss, A.**, **Helgesen, G.**, **Kjærefjord, J.M.** and **Leith, D.A.** (2001) Sedimentology of the heterolithic and tide-dominated Tilje formation (Early Jurassic, Halten Terrace, Offshore Mid-Norway). In: *Norwegian Petroleum Society Special Publications* (Eds Martinsen, O.J. and Dreyer, T.), Vol. **10**, pp. 103–144. Elsevier, London.

Martinius, A.W., **Ringrose, P.S.**, **Brostrøm, C.**, **Elfenbein, C.**, **Næss, A.** and **Ringås, J.E.** (2005) Reservoir challenges of heterolithic tidal sandstone reservoirs in the Halten Terrace, mid-Norway. *Petrol. Geosci.*, **11**, 3–16.

Midtgaard, H.H. (1996) Inner-shelf to lower-shoreface hummocky sandstone bodies with evidence for geostrophic influenced combined flow, Lower Cretaceous, West Greenland. *J. Sed. Res.*, **66**, 343–353.

Morad, S., **Al–Ramadan, K.**, **Ketzer, J.M.** and **De Ros, L.F.** (2010) The impact of diagenesis on the heterogeneity of sandstone reservoirs: A review of the role of depositional facies and sequence stratigraphy. *AAPG Bull.*, **94**, 1267–1309.

Morton, N. (1965) The Bearreraig Sandstone Series (Middle Jurassic) of Skye and Raasay. *Scot. J. Geol.*, **1**, 189–216.

Morton, A., **Hallsworth, C.**, **Strogen, D.**, **Whitham, A.** and **Fanning, M.** (2009) Evolution of provenance in the NE Atlantic rift: The Early–Middle Jurassic succession in the Heidrun Field, Halten Terrace, offshore Mid-Norway. *Mar. Petrol. Geol.*, **26**, 1100–1117.

Müller, R., **Petter Ngstuen, J.**, **Eide, F.** and **Lie, H.** (2005) Late Permian to Triassic basin infill history and palaeogeography of the Mid-Norwegian shelf—East Greenland region. In: *Norwegian Petroleum Society Special Publications* (Eds Wandås, B.T.G., Nystuen, J.P., Eide, E. and Gradstein, F.), Vol. **12**, pp. 165–189. Elsevier, London.

Myrow, P.M. (1992) Bypass-zone tempestite facies model and proximality trends for an ancient muddy shoreline and shelf. *J. Sed. Res.*, **62**, 99–115.

Nichols, T.E., **Worden, R.H.**, **Houghton, J.E.**, **Griffiths, J.**, **Brostrøm, C.** and **Martinius, A.W.** (2025) Machine learning for reservoir quality prediction in chlorite-bearing sandstone reservoirs. *Geosciences*, **15**, 325.

Nishida, N., **Ito, M.**, **Inoue, A.** and **Takizawa, S.** (2013) Clay fabric of fluid-mud deposits from laboratory and field observations: Potential application to the stratigraphic record. *Mar. Geol.*, **337**, 1–8.

Nøttvedt, A. and **Kreisa, R.D.** (1987) Model for the combined-flow origin of hummocky cross-stratification. *Geology*, **15**, 357–361.

Odin, G. and **Fullagar, P.** (1988) Chapter C4 geological significance of the glaucony facies. In: *Developments in Sedimentology* (Ed Odin, G.S.), Vol. **45**, pp. 295–332. Elsevier, London.

Olariu, C. (2014) Autogenic process change in modern deltas. In: *From Depositional Systems to Sedimentary Successions on the Norwegian Continental Margin*, pp. 149–166. John Wiley & Sons, Hoboken.

Olariu, C., **Steel, R.J.**, **Dalrymple, R.W.** and **Gingras, M.K.** (2012) Tidal dunes versus tidal bars: The sedimentological and architectural characteristics of compound dunes in a tidal seaway, the lower Baronia Sandstone (Lower Eocene), Ager Basin, Spain. *Sed. Geol.*, **279**, 134–155.

Osman, A., **Steel, R.J.**, **Ramsook, R.** and **Olariu, C.** (2024) Impact of wave, tides and fluid mud on fluvial discharge

across a compound clinoform (Pliocene Orinoco Delta). *Sedimentology*, **71**, 1113–1148.

Pemberton, S.G. and **Gingras, M.K.** (2005) Classification and characterizations of biogenically enhanced permeability. *AAPG Bull.*, **89**, 1493–1517.

Pemberton, S.G., **MacEachern, J.A.**, **Gingras, M.K.** and **Saunders, T.D.A.** (2008) Biogenic chaos: Cryptobioturbation and the work of sedimentologically friendly organisms. *Palaeogeogr. Palaeoclimatol. Palaeoecol.*, **270**, 273–279.

Pham, V.T.H., **Lu, P.**, **Aagaard, P.**, **Zhu, C.** and **Hellevang, H.** (2011) On the potential of CO_2–water–rock interactions for CO_2 storage using a modified kinetic model. *Int. J. Greenh. Gas Con.*, **5**, 1002–1015.

Powell, J.H. (2010) Jurassic sedimentation in the Cleveland Basin: A review. *Proc. Yorks. Geol. Soc.*, **58**, 21–72.

Ramm, M. (1992) Porosity-depth trends in reservoir sandstones: Theoretical models related to Jurassic sandstones offshore Norway. *Mar. Petrol. Geol.*, **9**, 553–567.

Ramm, M. and **Bjørlykke, K.** (1994) Porosity/depth trends in reservoir sandstones: assessing the quantitative effects of varying pore-pressure, temperature history and mineralogy, Norwegian shelf data. *Clay Mineral.*, **29**, 475–490.

Reesink, A.J.H. and **Bridge, J.S.** (2007) Influence of superimposed bedforms and flow unsteadiness on formation of cross strata in dunes and unit bars. *Sed. Geol.*, **202**, 281–296.

Reesink, A.J.H. and **Bridge, J.S.** (2009) Influence of bedform superimposition and flow unsteadiness on the formation of cross strata in dunes and unit bars – Part 2, further experiments. *Sed. Geol.*, **222**, 274–300.

Reynaud, J.-Y. and **Dalrymple, R.W.** (2012) Shallow-marine tidal deposits. In: *Principles of Tidal Sedimentology* (Eds Davis, R.A., Jr. and Dalrymple, R.W.), pp. 335–369. Springer, Netherlands.

Rossi, V.M. and **Steel, R.J.** (2016) The role of tidal, wave and river currents in the evolution of mixed-energy deltas: Example from the Lajas Formation (Argentina). *Sedimentology*, **63**, 824–864.

Rossi, V.M., **Perillo, M.M.**, **Steel, R.J.** and **Olariu, C.** (2017) Quantifying mixed-process variability in shallow-marine depositional systems: What are sedimentary structures really telling us? *J. Sed. Res.*, **87**, 1060–1074.

Saïag, J., **Brigaud, B.**, **Portier, É.**, **Desaubliaux, G.**, **Bucherie, A.**, **Miska, S.** and **Pagel, M.** (2016) Sedimentological control on the diagenesis and reservoir quality of tidal sandstones of the Upper Cape Hay Formation (Permian, Bonaparte Basin, Australia). *Mar. Petrol. Geol.*, **77**, 597–624.

Scotese, C.R., **Song, H.**, **Mills, B.J.W.** and **van der Meer, D.G.** (2021) Phanerozoic paleotemperatures: The earth's changing climate during the last 540 million years. *Earth Sci. Rev.*, **215**, 103503.

Sokkel Direktoratet (SODIR). (2025) Open data. Norwegian Offshore Directorate. https://www.sodir.no/en/facts/data-and-analysis/open-data/.

Sundal, A. and **Hellevang, H.** (2019) Using reservoir geology and petrographic observations to improve CO_2 mineralization estimates: Examples from the Johansen Formation, North Sea, Norway. *Minerals*, **9**, 671.

Surlyk, F., **Alsen, P.**, **Bjerager, M.**, **Dam, G.**, **Engkilde, M.**, **Hansen, C.F.**, **Larsen, M.**, **Noe-Nygaard, N.**, **Piasecki, S.**, **Therkelsen, J.** and **Vosgerau, H.** (2021) Jurassic stratigraphy of East Greenland. *GEUS Bull.*, **46**, 6521.

Taylor, A.M. and **Goldring, R.** (1993) Description and analysis of bioturbation and ichnofabric. *J. Geol. Soc. London*, **150**, 141–148.

Thrana, C., **Næss, A.**, **Leary, S.**, **Gowland, S.**, **Brekken, M.** and **Taylor, A.** (2014) Updated depositional and stratigraphic model of the Lower Jurassic Åre Formation, Heidrun Field, Norway. In: *From Depositional Systems to Sedimentary Successions on the Norwegian Continental Margin* (Eds Martinius, A.W., Råvnas, R., Howell, J.A., Steel, R.J. and Wonham, J.P.), pp. 253–289. John Wiley & Sons, Hoboken.

Virolle, M., **Brigaud, B.**, **Bourillot, R.**, **Féniès, H.**, **Portier, E.**, **Duteil, T.**, **Nouet, J.**, **Patrier, P.** and **Beaufort, D.** (2019a) Detrital clay grain coats in estuarine clastic deposits: origin and spatial distribution within a modern sedimentary system, the Gironde Estuary (south-west France). *Sedimentology*, **66**, 859–894.

Virolle, M., **Brigaud, B.**, **Luby, S.**, **Portier, E.**, **Féniès, H.**, **Bourillot, R.**, **Patrier, P.** and **Beaufort, D.** (2019b) Influence of sedimentation and detrital clay grain coats on chloritized sandstone reservoir qualities: Insights from comparisons between ancient tidal heterolithic sandstones and a modern estuarine system. *Mar. Petrol. Geol.*, **107**, 163–184.

Walderhaug, O. (1996) Kinetic modeling of Quartz cementation and porosity loss in deeply buried sandstone reservoirs. *AAPG Bull.*, **80**, 731–745.

Wooldridge, L.J., **Worden, R.H.**, **Griffiths, J.** and **Utley, J.E.P.** (2017) Clay-coated sand grains in petroleum reservoirs: Understanding their distribution via a modern analogue. *J. Sed. Res.*, **87**, 338–352.

Wooldridge, L.J., **Worden, R.H.**, **Griffiths, J.**, **Utley, J.E.P.** and **Thompson, A.** (2018) The origin of clay-coated sand grains and sediment heterogeneity in tidal flats. *Sed. Geol.*, **373**, 191–209.

Worden, R.H. and **Morad, S.** (2003) Clay minerals in sandstones: Controls on formation, distribution and evolution. In: *Clay Mineral Cements in Sandstones*, pp. 1–41. John Wiley & Sons, Hoboken.

Worden, R.H., **Griffiths, J.**, **Wooldridge, L.J.**, **Utley, J.E.P.**, **Lawan, A.Y.**, **Muhammed, D.D.**, **Simon, N.** and **Armitage, P.J.** (2020) Chlorite in sandstones. *Earth Sci. Rev.*, **204**, 103105.

Manuscript received 29 August 2025; revision accepted 24 February 2026

Supporting Information

Additional information may be found in the online version of this article:

Table S1. Observed lithofacies of the Tilje Formation, based on descriptions of lithology, grain size, sorting, sedimentary structures and trace fossils.